SURFACE AND INTERFACE ANALYSIS
Surf. Interface Anal. 2004; **36**: 1269–1303
Published online 1 September 2004 in Wiley InterScience (www.interscience.wiley.com). DOI: 10.1002/sia.1909

SIA

Critical review of the current status of thickness measurements for ultrathin SiO_2 on Si Part V: Results of a CCQM pilot study

M. P. Seah,[1]* S. J. Spencer,[1] F. Bensebaa,[2] I. Vickridge,[3] H. Danzebrink,[4] M. Krumrey,[5] T. Gross,[6] W. Oesterle,[7] E. Wendler,[8] B. Rheinländer,[9] Y. Azuma,[10] I. Kojima,[10] N. Suzuki,[11] M. Suzuki,[12] S. Tanuma,[13] D. W. Moon,[14] H. J. Lee,[15] Hyun Mo Cho,[16] H. Y. Chen,[17] A. T. S. Wee,[18] T. Osipowicz,[19] J. S. Pan,[20] W. A. Jordaan,[21] R. Hauert,[22] U. Klotz,[22] C. van der Marel,[23] M. Verheijen,[23] Y. Tamminga,[24] C. Jeynes,[25] P. Bailey,[26] S. Biswas,[27] U. Falke,[28] N. V. Nguyen,[29] D. Chandler-Horowitz,[29] J. R. Ehrstein,[29] D. Muller[30] and J. A. Dura[31]

(see Appendix for addresses)

Received 7 January 2004; Revised 29 March 2004; Accepted 29 March 2004

Results are reported from a pilot study under the Consultative Committee for Amount of Substance (CCQM) to compare measurements of and resolve any relevant measurement issues in the amount of thermal oxide on (100) and (111) orientation silicon wafer substrates in the thickness range 1.5–8 nm. As a result of the invitation to participate in this activity, 45 sets of measurements have been made in different laboratories using 10 analytical methods: medium—energy ion scattering spectrometry (MEIS), nuclear reaction analysis (NRA), RBS, elastic backscattering spectrometry (EBS), XPS, SIMS, ellipsometry, grazing—incidence x-ray reflectometry (GIXRR), neutron reflectometry and transmission electron microscopy (TEM). The measurements are made on separate sets of 10 carefully prepared samples, all of which have been characterized by a combination of ellipsometry and XPS using carefully established reference conditions and reference parameters.

The results have been assessed against the National Physical Laboratory (NPL) data and all show excellent linearity. The data sets correlate with the NPL data with average root-mean-square scatters of 0.15 nm, half being better than 0.1 nm and a few at or better than 0.05 nm. Each set of data allows a relative scaling constant and a zero thickness offset to be determined. Each method has an inherent zero thickness offset between 0 nm and 1 nm and it is these offsets, measured here for the first time, that have caused many problems in the past. There are three basic classes of offset: water and carbonaceous contamination equivalent to ~1 nm as seen by ellipsometry; adsorbed oxygen mainly from water at an equivalent thickness of 0.5 nm as seen by MEIS, NRA, RBS and possibly GIXRR; and no offset as seen by XPS using the Si 2p peaks. Each technique has a different uncertainty for the scaling constant and consistent results have been achieved. X-ray photoelectron spectroscopy has large uncertainties for the scaling constant but a high precision and critically, if used correctly, has zero offset. Thus, a combination of XPS and the other methods allows the XPS scaling constant to be determined with low uncertainty, traceable via the other methods. The XPS laboratories returning results early were invited to test a new reference procedure. All showed very significant improvements. The reference attenuation lengths thus need scaling by 0.986 ± 0.009 (at an expansion factor of 2), deduced from the data for the other methods. Several other methods have small offsets and, to the extent that these can be shown to be constant or measurable, these methods will also show low uncertainty. Recommendations are provided for parameters for XPS, MEIS, RBS and NRA to improve their accuracy. © Crown Copyright 2004. Reproduced by permission of the Controller of HMSO.

KEYWORDS: calibration; ellipsometry; gate oxides; GIXRR; interlaboratory study; MEIS; neutron reflectometry; NRA; RBS; silicon dioxide; SIMS; TEM; thickness measurement; traceability; XPS

*Correspondence to: M. P. Seah, Division of Quality of Life, National Physical Laboratory, Teddington, Middlesex TW11 0LW, UK.
E-mail: martin.seah@npl.co.uk
Contract/grant sponsor: UK Department of Trade and Industry.

INTRODUCTION

The system of an ultrathin layer of SiO_2 on the surface of Si has been chosen, here, as both an important system *per se* and also as an archetypal system for study by a wide range of methods in order to evaluate their measurement uncertainty. This system is one of the most intensively studied ultrathin layer systems that is readily available. A major effort has been made in the past arising from the use of SiO_2 as a gate oxide and, more latterly, as an ultrathin gate oxide. The availability of silicon wafers as substrates for other work where functional layers are deposited for sensors and also the availability of significant quantities of ultrapure Si to fabricate artefacts both lead to ongoing needs to understand and measure this system. This work is for thermally grown oxides on Si. Oxides formed by other routes, such as by polishing, chemical vapour deposition or by wet processing may give significantly different results.

The International Technology Roadmap for Semiconductors (ITRS)[1] indicates a need for analysis in, and the measurement of, ultrathin gate oxides at a control uncertainty of better than 4%, but this is for an expansion factor of 3 in the uncertainty, so the standard uncertainty is just over 1%. In the analysis of thin layers by electron spectroscopies such as Auger electron spectroscopy (AES) or x-ray photoelectron spectroscopy (XPS) there is a dominant uncertainty of 10%[2] to 17.4%[3] arising from the critical parameter, the inelastic mean free path, where direct calculations are available, or 20.4%[4] if the generic equation, known as TPP-2M,[5] is used. Few studies using traditional surface analytical techniques have ever claimed high accuracies for measurement because of this uncertainty and this has inhibited progress.

Analyses of thickness determinations by XPS show that, provided that proper care is taken in the analysis, the linearity of simple equations is valid for the 0.5–8 nm range to within ±0.025 nm.[6] This linearity may be achieved only if the counting system is linear[7,8] and if the software to remove the backgrounds and conduct the peak area analysis is valid.[9] If either of these functions is not correct, errors may occur. Unfortunately, today there are many 'functioning' systems in laboratories where these problems are significant but are undiagnosed.

In addition to the electron methods of AES and XPS are the ion methods of medium-energy ion scattering spectrometry (MEIS), Rutherford backscattering spectrometry (RBS) and secondary ion mass spectrometry (SIMS), which have possibilities to reach uncertainties as low as 2% but have issues needing study that are different from those of AES and XPS. Both MEIS and RBS are intrinsically more linear and have higher general accuracy than AES and XPS through their stopping powers or relevant cross-sections. On the other hand, there are layer thickness measuring methods using wave interference effects that should reach 2% or better but do not have the analytical power of the spectroscopies. In this work, we shall intercompare these and other methods. The methods selected are those thought to be important by analysts responding to an invitation to participate in this pilot study under the auspices of the Consultative Committee for Amount of Substance (CCQM).[10] This committee is the body authorized under the International Committee for Weights and Measures (CIPM)[11] to oversee the framework for the SI system in relation to measures of amount of substance. The invitation was made by all delegates to the CCQM, by searches of National Measurement Institute (NMI) activity via the web and by a number of experts known to be involved in the measurement of SiO_2 on Si thicknesses. Samples were then posted from the beginning of March 2002.

In this work we are concerned with ultrathin layers at a free surface. In the preparation of electronic devices these layers may be buried under other layers, such as the gate or other capping materials. Determination of the thicknesses of these layers may not be made by all of the present methods and so the conclusions we present later may or may not be appropriate for that situation. Additionally, often one needs other attributes, such as extreme localization, that would favour transmission electron microscopy (TEM), or speed and the absence of vacuum constraints that would favour ellipsometry. These issues are not part of this study. As described later, the present samples are prepared by thermal oxidation and so the results are strictly relevant to this very simple and rather ideal system. The extent of the interfacial oxides is shown to be the minimum compatible with a bonded interface. Oxides may be grown also by plasma and other methods and then the extent of the interfacial oxides and the oxide density may differ from that used here. Oxides also may be formed at mechanically polished silicon surfaces that may involve additional hydroxides and mechanically damaged interfaces. For all these other films some of the methods reported here may be used directly but other methods may need further consideration concerning changes in composition, density, interfacial oxides and film unevenness in order to obtain comparable accuracy to the thickness data reported here.

Many intercomparisons have been made in the past[12–16] for the thickness of layers of thermal SiO_2 at the surface of Si and a recent study to establish current working practice in analytical laboratories[14] gave the results shown in Fig. 1. The present work focuses on the thickness range 1.5–8 nm.

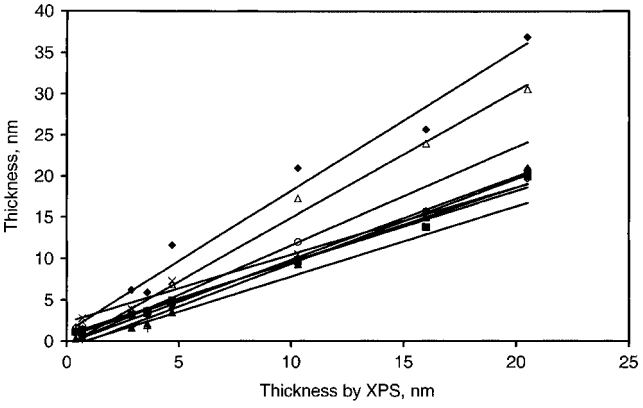

Figure 1. Data for measurement of the thicknesses of thin layers of SiO_2 on Si by different methods, after Cole *et al*.:[14] (■) RBS; (▲) quadrupole SIMS; (△) capped sample with magnetic sector SIMS; (♦) capped sample with quadrupole SIMS; (◊) capped sample with quadrupole SIMS using different criterion; (●) XPS; (+) AES; (×) ellipsometry; (○) TEM.

In Fig. 1 we see a spread in the measured thicknesses from 9 nm to 21 nm at 10 nm thicknesses, from 1.6 nm to 6.2 nm at 3 nm thicknesses and from 0.2 nm to 2.8 nm at 0.7 nm thicknesses. The errors tend to bias the data towards greater thickness and these can exceed 100%. The authors conclude that TEM, XPS, AES, SIMS, RBS and ellipsometry can measure qualitative differences in thicknesses but that each is best in certain thickness ranges and no method is accurate across the entire range. In the work of Lu *et al.*,[12] spectroscopic ellipsometry, TEM and electrical capacitance–voltage measurements are compared and good correlations are found at 2 nm, with the range being from 1.8 to 2.2 nm; this range did not degrade significantly for thicker samples. The electrical thickness was justified to be slightly greater than for the other methods. In the analysis by Richter *et al.*,[13] spectroscopic ellipsometry neutron reflectometry and grazing-incidence x-ray reflectometry (GIXRR) are compared at 10 nm thickness. This analysis differed from those above in that one sample was analysed by the three methods in one NMI laboratory, with iteration of the analytical model to ensure consistency. In this case the data fell into the range 10.17–10.27 nm, which was an excellent result. In the work of Semak *et al.*,[15] the Tougaard method for XPS,[17,18] angle-resolved XPS (ARXPS), RBS and ellipsometry were compared and the Tougaard and ARXPS data were analysed using Tougaard's software packages.[19] The XPS approaches were found to be consistent but the deviation between the other techniques was significantly larger (~30–40%). In the work of Chang *et al.*,[16] MEIS, TEM, spectroscopic ellipsometry and the electrical methods of current–voltage and capacitance–voltage are compared. They conclude that all methods agree within a range of 0.6 nm (±0.3 nm) for thicknesses between 2 and 9 nm.

In the studies outlined above there is considerable and useful discussion of the issues of uncertainty. In three of the studies there was more possibility for convergence because work could be iterated in small groups of scientists in regular collaboration. In Cole *et al.'s* study,[14] analysts using different methods in one company reported results independently to establish capability, which is probably the fairest reflection of general analytical practice. In the present work we will show how this can be improved and what the present best current interpretational practice is, building on these earlier studies.

In analysing this problem, we adopt the model for the oxide shown in Fig. 2. We shall not consider interface roughnesses unless specifically noted. The surface roughness, measured by atomic force microscopy (AFM), was typically <0.1 nm. Separate samples are studied by each laboratory and only in a few cases are these samples subjected to a second analysis using a different method either in that laboratory or by colleagues from an associated laboratory. The samples are of thermal oxide on (100) or (111) Si wafers and are contaminated by a layer of carbonaceous contamination after manufacture.[21] At the interface between the oxide and the substrate there will be suboxides, simply because the outermost layer of the substrate Si atoms has an environment that contains oxygen from the SiO_2, but this of course will not have the stoichiometry of SiO_2. The extent to which this model is valid will become clear as we analyse the data.

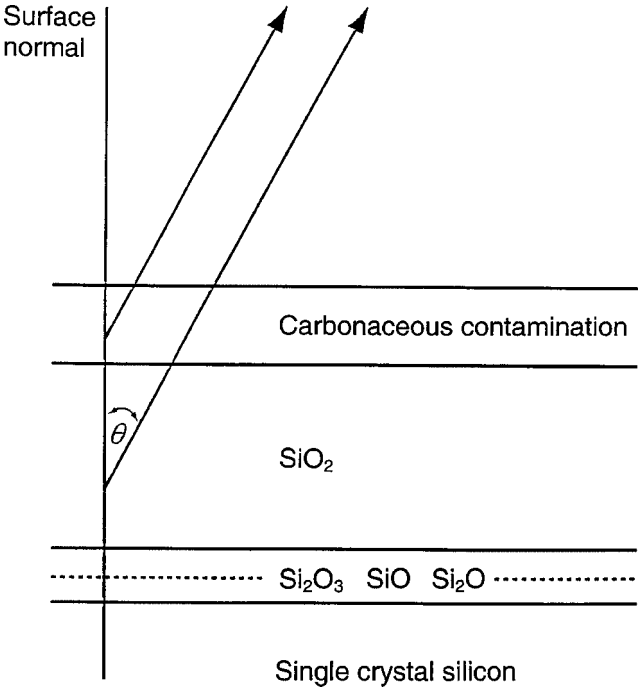

Figure 2. Model of the oxide surface, after Seah and Spencer.[20] All angles in this study are referenced to the surface normal.

We may measure the amount of SiO_2 on the Si by methods that give the amount of substance or by methods that give the layer thickness. These measures will be related by the SiO_2 density, ρ_{SiO_2}. There are various values for the density in the literature, ranging from 2.650 g cm^{-3} for α-quartz[22,23] to 2.196 g cm^{-3} for vitreous or amorphous quartz or thermal SiO_2.[24] In this work, the value of 2.196 g cm^{-3} will be used as a consistent and commonly accepted value for the thermal oxide to help homogenize the data from different laboratories. We shall return to this point later in this study.

Variations will be found between the thicknesses determined in different laboratories using different analytical methods and these variations arise from: the different physics of the methods, leading to measurements of a slightly different property; differences between laboratories using the same method but analysing the experimental data, such as intensities, differently; differences in the calculations, leading to different evaluations of the thicknesses; differences in the values of associated input parameters; and small differences arising from analytical precision. There are two further important aspects that affect results. The first of these is calculational error. In this study we encountered errors of up to a factor of 2 from transcription, calculation or erroneous input values, but these have been removed, as far as we can tell, from the data reported here. The second arises from the analysis, by different laboratories, of different samples, as is the case with most of these studies, rather than each laboratory analysing the same set of samples in turn. We therefore needed to consider the choice of samples very carefully.

In principle, the methods involving traceability to thickness expressed as length would be expected to be the

most accurate but the thickness determined as atoms m^{-2} can be more meaningful and is often, but not always, the measure that is needed by users. The reason for this arises because the meaning of length in relation to materials becomes ill-defined below 0.05 nm. Changes in length are meaningful. We can say that a metre bar has expanded by 0.001 nm because we may take any reference point and compare the positions before and after heating. However, to say that this metre bar or this row of atoms is a particular length requires us to be able to define where in the electron cloud distribution we shall take the effective edge of the relevant atoms to be. This is not possible at the present time. This problem is automatically dealt with for the measurements in terms of atoms m^{-2} because each atom has a probability of being detected. We shall see later how this concern for the measuring of thickness, in terms of length, may be partly circumvented. Despite the fact that it is atoms m^{-2} that is meaningful, we shall work in terms of length with an exact conversion via the above density of the thermal SiO_2. The reason for this is that, at the present time, analysts understand the limitations of measurements at the monolayer or nanometre level but most would not immediately be able to relate this to be either more or less than a number such as, say, 10^{20} atoms m^{-2} (this is actually ~6.12 monolayers of SiO_2, as discussed in the Results section).

The analytical methods employed in this study were MEIS, nuclear reaction analysis (NRA), RBS and the related technique of elastic (non-Rutherford) backscattering spectrometry (EBS), SIMS and XPS. Even where the results from these methods are expressed in units of length, the actual measure implicit in most of these methods is in units of atoms m^{-2}. The methods that give length are GIXRR, neutron reflectometry and TEM. Other methods using optics are ellipsometry and spectroscopic ellipsometry. The distribution of methods over countries is shown in Table 1. An excellent review covering these and other methods for measuring thin gate oxide films is given by Diebold *et al*.[25]

The reasons for including this wide range of methods are important. The methods of MEIS, RBS and EBS are analytical and can measure the number of atoms per unit area from the backscattered ion energy spectrum peak area, or alternatively the thickness may be determined from the rate of energy loss of the ions and the energy width of that peak. In this mode MEIS gives a density-dependent thickness measure that is constant in terms of the amount of substance. By using channelling directions of the substrate for both the incident beam and the scattered and detected particles, the general background from the substrate may be reduced in MEIS. For RBS and EBS, only channelling of the incident beam is necessary to do this. This improves the measurement precision. With MEIS, the sensitivity is generally higher than for RBS and the energy loss in the sample is measured more easily. Uncertainties arise from the required rate of energy loss and the system geometric parameters. On the other hand, there are more RBS instruments in service and there is greater experience in RBS measurements. Uncertainties arise from the beam fluence and the system geometric parameters. The RBS sensitivity may be improved by using resonance conditions to give an enhanced, non-Rutherford cross-section, and then the method becomes EBS. Now the uncertainties arise from the beam fluence, system geometry and the cross-section. Nuclear reaction analysis uses a beam of 860 keV deuterons to probe the nuclear reaction $^{16}O(d,p_1)^{17}O^*$ in order to detect oxygen with great sensitivity. It therefore also gives the oxygen thicknesses in terms of atoms per unit area via a calibrated reference sample. Nuclear reaction analysis is popular for oxygen because it gives good signal quality and is linear to thicknesses of >100 nm.

Secondary ion mass spectrometry was chosen because it is important for industrial measurements of these layers, particularly layers that are not homogeneous, such as the ultrathin oxynitrides of silicon and where the precise distribution of the nitrogen in the layer is required. Secondary ion mass spectrometry is not expected to be as precise or accurate as the other methods for SiO_2 but has important uses for post-SiO_2 gate oxides. It was therefore decided to include it to assess relevant measurement issues here. X-ray photoelectron spectroscopy is the main surface analysis method for layers <10 nm thick and has advantages over RBS and MEIS in that the equipment is smaller and allows the amount of elements in different chemical states to be

Table 1. The numbers of instruments used by country in the study

	Spectroscopy					Length			
Country	MEIS	NRA	RBS	SIMS	XPS	Ellipsometry	GIXRR	Neutron reflectometry	TEM
Canada					1				
France		1							
Germany			1		1	2	1		2
Japan					2	1	1		
Korea	1					1			1
Netherlands			1		2				1
Singapore			1		3	1			
South Africa					1				
Switzerland					1				1
UK	1		1	1	1	1			1
USA						2		1	1

determined. Methods that measure the total oxygen present will also measure the quantity of oxygen in any carbonaceous contamination or adsorbed water layers. However, XPS can measure simply the amount present as SiO_2. Of course, RBS can measure quantities at depths far beyond the measurement depth of XPS and so has application to thicknesses of >100 nm, with generally high detectabilities and low uncertainties for many important elements.

The wavelength interference methods of GIXRR and neutron reflectometry both probe the film thickness using interference between waves scattered from the upper and lower surfaces of the oxide film. These require much flatter and larger samples than the analytical methods but provide a more direct traceability to length via the wavelengths of the radiations used. These are particularly popular in the 10–100 nm range where the measurement precision is very good. Transmission electron microscopy is used with cross-sections of the oxide in which the Si substrate lattice is also imaged with columns of Si atoms to provide the length calibrations of each image traceably to the Si lattice spacing. This spacing is known to better than 1 ppm if the temperature is known. Transmission electron microscopy is popular for this very direct traceability. New automated sample preparation methods using focused ion beams, are increasing the applicability of TEM. Ellipsometry has similarities to GIXRR and neutron reflectometry but, using longer wavelengths, does not provide interference minima and maxima. Instead, the phase shift and polarization rotation are measured and, from these and the optical constants of the material of the film, the film thickness is calculated. This method is probably the fastest and most economic of all the methods, as well as having the greatest precision. It is therefore used as a metrology tool in water fabrication facilities.

Thus, in the techniques selected above we have methods that have very high precision, measurements of the amount of oxygen, measurements of the amount of SiO_2, measurements of length traceable to accurately known wavelengths or the Si lattice and methods that are readily extended to other systems. Each method has both strengths and weaknesses that we shall evaluate in this study but the complementariness of the techniques allows their true strengths to be defined.

Bearing in mind that ellipsometry and XPS can measure these oxides with precisions of better than 1%,[26] it was decided to provide analysts in this study with samples that were characterized to better than 1%. The preparation of the samples is described in the next section.

PREPARATION OF THE SAMPLES

There is significant comment in different articles attributing the differences observed in experiments to differences between the properties of the samples fabricated or analysed in the different laboratories. To check if the data were source dependent, we obtained materials from two different suppliers specializing in ultrathin gate oxide manufacture, one in the USA and one in Europe. The materials from the USA were a set of eight 200 mm (100) wafers from which two were selected. The European material was in the form of a set of sixty 100 mm wafers from which four (100) wafers and four (111) wafers were selected. These were sufficient for the intended study but, as extra participants were added, extra samples were cut from additional wafers. Both (100) and (111) Si wafers were used to check in case any problems arose through the orientation of the substrate on which the oxide is grown. The rate of growth of the oxide is known to be different for these surfaces at these thicknesses,[27,28] but the oxide itself is thought to be the same. All material was grown by thermal oxidation in furnaces designed for ultrathin gate oxides to generate several wafers at each of a number of thicknesses in the range 1.5–8 nm. The US material was provided in a sealed dust-free container to the European facility where all of the samples were mapped for the oxide thickness using a Philips PZ 2000 ellipsometer designed for production line thickness determination. This instrument provided maps with a precision of ~0.002 nm, allowing samples to be selected from regions that were homogeneous to 1%. An example of a map, in colour, is given in plate 1 of Ref. 26. That particular example shows a central region of 80 mm diameter that could have been used but other samples were more homogeneous and so were used instead.

To ensure the best accuracy, the thickness of each sample provided to analysts was recorded for its position in each ellipsometry map. The ten thicknesses chosen for this study were six of Si(100), being of nominal thicknesses 2, 3, 4, 4.5, 5 and 8 nm, together with four of Si(111), being of nominal thicknesses 2, 4, 6 and 7 nm. The Si(100) wafers were cut into squares bounded by the (111) planes defining the [110] directions, whereas the (111) wafers were cut into triangles bounded by the same planes and directions.[20]

After cutting, the samples were blown with an argon jet to remove cutting debris and then most of the carbonaceous contamination was removed by a careful washing procedure involving repeated washes in isopropyl alcohol, ultrasonic agitation in fresh isopropyl alcohol and blow drying with an argon jet. In this way, the thickness of the remaining carbon could be reduced from typically 0.64 nm to a layer 0.18 nm thick.[21] Subsequent tests of storage in different containers showed that the contamination thickness increased with the square root of time and that polypropylene 'Fluoroware' would typically keep this below 0.25 nm for 3 months.[21] Samples therefore were supplied in these containers, only to be opened just prior to use. The carbonaceous contamination thicknesses evaluated above were measured by XPS and calculated for attenuation lengths based on an average polymer and not glassy carbon. Use of glassy carbon data is incorrect and would lead to erroneous values a factor of 2 lower.[21]

In addition to the growth of the carbonaceous contamination, repeat XPS measurements of the oxide thicknesses have been made for one set of the samples stored in the Fluoroware containers after 6 months. The average increase in thickness over the 6 months is 0.001 ± 0.059 nm. The samples are thus assumed to be stable for the period of the measurements reported here. The samples were despatched from March 2002.

By preparing a very large number of samples so that each laboratory analysed a fresh sample, the possibilities of further contamination were significantly reduced. In only two cases were samples analysed in one laboratory and then passed to colleagues using another method in the same laboratory. In one of these cases, but in no others, contamination by other elements was measured but the contamination was too low to affect the results significantly.

INSTRUCTIONS TO ANALYSTS

The instructions to analysts included methods for cleaning the samples in case an accident occurred. This was not needed and all samples were analysed 'as received'. Analysts were asked to measure all ten samples and, if they had time, to repeat this and then repeat the measurement on the 5 nm (100) sample a further six times, removing it from the analytical position and replacing it each time. This would provide a measure of the sample-to-sample repeatability. Analysts were asked to evaluate the thicknesses and report their evaluation of the uncertainties according to the Guide to the Expression of Uncertainty in Measurement.[29] Having reported the thicknesses, analysts were asked for tables of the experimental intensities or other data in order to be able to calculate the thickness values independently, where practicable. For the more time-consuming methods of GIXRR, neutron reflectometry and TEM, analysts rarely measured data for all ten samples but measured as many as they could.

In the early stages of this work, while analysts were conducting their measurements, it became clear that in XPS significant uncertainties could occur for those making measurements at emission angles associated with low index directions, where forward focusing would enhance the substrate signal.[20] Additionally, those conducting angle-resolved XPS measurements could find a bias introduced, depending on how they interpreted the data.[6] Those returning XPS data were therefore invited to repeat the measurements using a reference geometry of just one fixed angle of emission in a defined azimuth.[20] These invitations were from July 2002. This reference geometry was 34° from the surface normal in an azimuth at 22.5° to one of the edges of the square (100) samples or at 25.5° from the surface normal in an azimuth of one of the edges of the triangular (111) samples, as shown in Fig. 3. Eleven sets of XPS data were provided for the reference geometry.

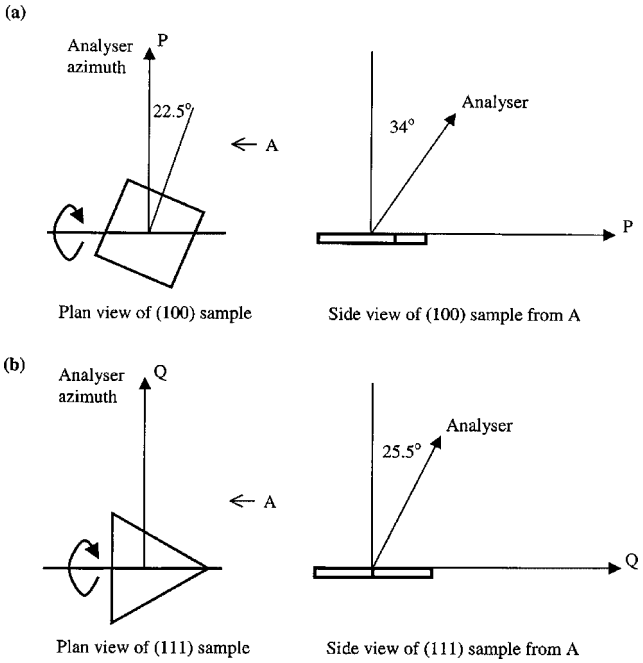

Figure 3. Geometry of the XPS reference conditions: (a) (100) surfaces with the angle of emission at 34° from the surface normal and the analyser set in an azimuth of the square Si sample that is in its surface and at 22.5° to the direction of one of the edges; (b) (111) surfaces with the angle of emission at 25.5° from the surface normal and the analyser set in an azimuth of the triangular Si sample that is in its surface and parallel to the direction of one of the edges.

RESULTS AND DISCUSSION

Method for evaluating the results

The method of expressing the analysis simply, and the justification of the approach used, really only become evident when the data have been analysed. To simply provide distributions or values of the thicknesses with the individual evaluations of uncertainties obtained for each material would drown the reader in undigested detail. We shall see that the current approach rapidly allows us to focus on the essential issues.

To provide a reference for each sample, the thicknesses of one sample from each wafer were measured by XPS on two separate occasions and the average thickness was determined. Details of the generic spectra and the measurement method are given in Ref. 20. Briefly, the XPS system is a VG Escalab II with five channel electron multipliers, with the angle γ between the Mg x-ray source and the spectrometer set at the magic angle of 54.7°. The samples were set at the reference geometry and details of the Si 2p peak were recorded. For spectral analysis, the x-ray satellites were removed together with the $2p_{3/2,1/2}$ spin-orbit splitting determined as 50% of the intensity at 0.60 eV higher binding energy.[30] The remaining structure was evaluated as five peak intensities: I_{Si} and I_{Si_2O} at 0.95 eV higher binding energy (BE), I_{SiO} at 1.75 eV higher BE, $I_{Si_2O_3}$ at 2.48 eV higher BE and I_{SiO_2} at 3.96–4.36 eV higher BE, as defined by Hollinger and Himpsel[30] and by Keister *et al.*[31] These peaks were fitted with peak positions fixed, as indicated, in relation to the Si peak, except for the SiO_2 peak that was allowed to move to higher BE as the film thickness increased. The peak fitting was simultaneous with the removal of a Shirley background,[32] with a fifteen-point smooth inwards from the end points at 8.2 eV higher and 2.7 eV lower BE than the Si 2p peak. All peak full widths at half-maxima (FWHMs) were constrained to be in the range 0.7–1.5 eV.

Figure 4 gives an illustrative widescan spectrum and details of the Si 2p peak region.[20] The thickness d of the oxide may be calculated using the well-known relation for photoelectrons from the metal and oxide states of a

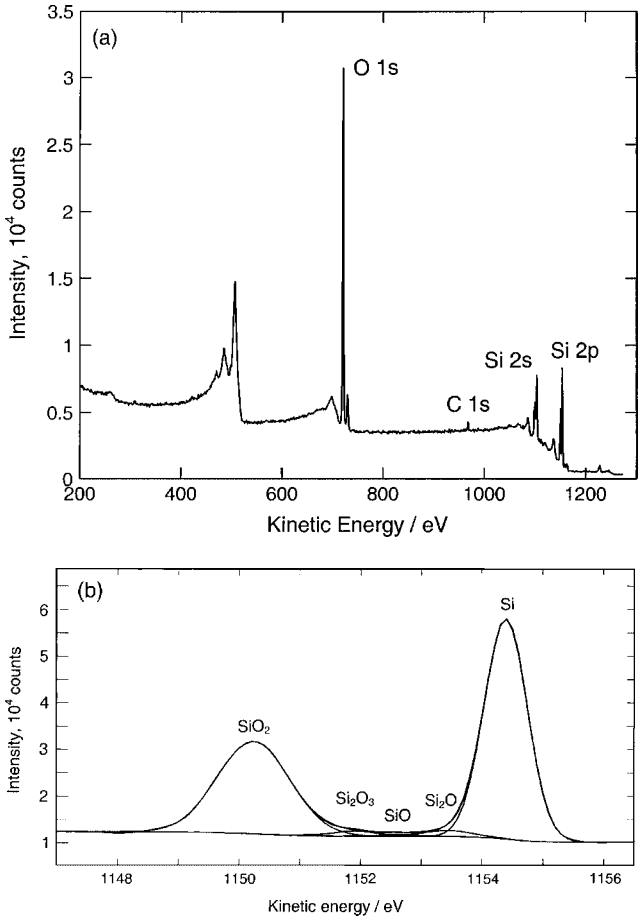

Figure 4. The XPS spectra using Mg x-rays for a sample with ~2 nm of oxide after cleaning: (a) widescan; (b) the Si 2p peaks after satellite removal, spin-orbit removal and peak fitting with a single Shirley background, after Seah and Spencer.[20]

single peak

$$d = L\cos\theta \ln(1 + R_{expt}/R_o) \quad (1)$$

where d is the oxide thickness, L is the attenuation length of the substrate and oxide photoelectrons in the oxide, R_{expt} is the ratio of the measured intensities of the photoelectrons from the oxide and the elemental states from the sample and R_o is the ratio of these intensities from bulk materials. From Fig. 2 we see that there are intermediate oxides and a carbonaceous overlayer. Fortunately, the latter has no effect.[20] The intermediate oxides, however, mean that we should really replace Eqn. (1) by the following four equations[6]

$$d_{SiO_2} = L_{SiO_2}\cos\theta \times \ln\left[1 + \frac{\left(\frac{I_{SiO_2}}{R_{SiO_2}}\right)}{\left(\frac{I_{Si_2O_3}}{R_{Si_2O_3}} + \frac{I_{SiO}}{R_{SiO}} + \frac{I_{Si_2O}}{R_{Si_2O}} + I_{Si}\right)}\right] \quad (2)$$

$$d_{Si_2O_3} = L_{Si_2O_3}\cos\theta \ln\left[1 + \left(\frac{I_{Si_2O_3}}{R_{Si_2O_3}I_{Si}}\right)\right] \quad (3)$$

$$d_{SiO} = L_{SiO}\cos\theta \ln\left[1 + \left(\frac{I_{SiO}}{R_{SiO}I_{Si}}\right)\right] \quad (4)$$

$$d_{Si_2O} = L_{Si_2O}\cos\theta \ln\left[1 + \left(\frac{I_{Si_2O}}{R_{Si_2O}I_{Si}}\right)\right] \quad (5)$$

We then sum these thicknesses to give the effective oxide thickness using the relation

$$d_{oxide}(5P) = d_{SiO_2} + 0.75d_{Si_2O_3} + 0.5d_{SiO} + 0.25d_{Si_2O} \quad (6)$$

which apportions the thickness according to the oxygen content. The 5P in parentheses is simply to distinguish the value from this equation from that using Eqn. (1) in which only the peaks for Si and SiO_2 are used. For the above method and calculations it may be shown, using fuller theory with elastic scattering, that Eqns (1)–(5) are linear and valid within ±0.025 nm over the 0.3–8 nm thickness range covered here.[6] From measurements elsewhere,[6] R_{SiO_2} is 0.9329 ± 0.02 and, of course, R_{Si} is unity. Note that if a different type of background had been selected for removal, the value of R_{SiO_2} would change. Calculations of the attenuation lengths, L_{SiO_2}, are given by Seah and Spencer[20] based on the inelastic mean free path (IMFP) value of Tanuma, Powell and Penn.[33] These attenuation length values are 2.964 nm for Mg Kα x-rays and 3.448 nm for Al Kα x-rays. The IMFP values on which these ALs are based are thought to be accurate to 17.4%.[3] The R and L values for the intermediate oxides are not known and so here we use a simple interpolation between the values for SiO_2 and Si. If this is not done, the calculated d_{oxide} values are increased by 0.007 ± 0.002 nm, which is an error well below the present measurement uncertainty.[6] The nominal values for the thicknesses of the wafers are given in Table 2. From two sets of measurements of the average for the ten basis NPL samples and two sets of measurements for a second set of samples, the difference between $d_{oxide}(5P)$ and d_{SiO_2}, as calculated above, is 0.128 ± 0.008 nm. This small difference is significant here and will be discussed below because these concepts are useful in the later analysis.

The intermediate oxides are formed at the interface of the SiO_2 and Si. It is useful, first, to consider a monolayer thickness for SiO_2. Using a value of 2.196 g cm^{-3} for the density of amorphous SiO_2[23] and a molecular weight for SiO_2 of 60.0843 amu, we find that there are 6.603×10^{28} atoms m^{-3} in the oxide, two-thirds of which are oxygen. On this basis, an average atom may be treated as a cube of side a, of volume a^3 and with a^{-3} atoms m^{-3}. Thus, a monolayer thickness may be treated as a layer 0.2474 nm thick containing 5.445×10^{18} Si atoms m^{-2} and 10.891×10^{18} O atoms m^{-2}. Similarly for the Si substrate with density 2.329 g cm^{-3} and molecular weight 28.0855 amu, there are 4.994×10^{28} atoms m^{-3} and, because the average Si monolayer thickness is 0.2716 nm, this contains 13.561×10^{18} Si atoms m^{-2}. The final layer of atoms of the SiO_2 at the Si interface has some oxygen, and therefore silicon, with Si_2O_3 coordination, some with SiO and some with Si_2O coordination. If these are, say, approximately equal

Table 2. Nominal thicknesses of the samples

	Substrate orientation									
	(100)						(111)			
Nominal thickness (nm)	2	3	4	4.5	5	8	2	4	6	7

in number, the equivalent SiO_2 thickness of these interfacial oxides is 0.2474 $\left(\frac{1}{3} \times \frac{3}{4} + \frac{1}{3} \times \frac{1}{2} + \frac{1}{3} \times \frac{1}{4}\right) = 0.124$ nm. If the interfacial oxides were all SiO the thickness would be $0.2474(1 \times \frac{1}{2})$, which gives the same result. This value is very close to the above value of 0.128 ± 0.008 nm for the equivalent SiO_2 thickness measured by XPS and indicates that the interface is probably as close to an abrupt interface, chemically, that could reasonably be attained in this system.

Repeat measures by XPS for an individual sample at different times show a repeatability standard deviation of 0.019 nm with repositioning of the sample. The stability of the samples is illustrated by results recorded at the start of the survey and after 6 months when most of the laboratories had returned data. The average growth in thickness of the samples was 0.001 ± 0.059 nm, where the latter is the standard deviation of the differences. In terms of the standard deviation of the mean, rather than the scatter of the data, the average thickness has increased by 0.001 ± 0.019 nm.

The difference between the samples measured by XPS at the NPL and the samples sent to the other laboratories was determined using the ellipsometry maps with a precision of better than 0.002 nm.[24] These maps were made soon after manufacture of the wafers and without them being released from their dust-free environments. The reference thickness, d_{RT}, for each sample sent to each laboratory was then taken as the value, by XPS, of the NPL samples given in Table 2, corrected for the small difference between the laboratory sample and the NPL reference sample as monitored by ellipsometry. The standard deviation of the distribution of material thickness from each wafer was typically 0.04 nm. The data returned to the NPL for the thicknesses of the samples were then plotted against their reference thicknesses and the result was fitted with a straight line of the form

$$d_{\text{respondee}} = m d_{RT} + c \qquad (7)$$

The constant c is the zero thickness offset (all thicknesses will be reported in nm) and represents an apparent layer thickness in excess of the reference thickness extrapolated to a d_{RT} value of zero. The gradient m is a scaling constant that should be approximately unity but may diverge from unity as a result of uncertainty in the measurements from the respondee laboratory or uncertainty in the d_{RT} value. It should be remembered that d_{RT} depends linearly on L_{SiO_2} and that this has a 17.4% type B uncertainty arising for values derived from the calculated IMFP. In addition to m and c we also evaluate r, the root-mean-square (rms) scatter of the data about the straight-line fit. To illustrate the use of Eqn. (7) we show in Fig. 5(a) the correlation of the ellipsometry data used for mapping the wafers and the NPL measurements by XPS. This plot gives a gradient m of 0.993 ± 0.016, an offset (or intercept) c of 0.480 ± 0.070 nm, where the uncertainties are standard uncertainties, and an rms scatter r of 0.089 nm. The intercept c, as discussed later, arises from the ellipsometry detecting the layers of contamination as part of the oxide. The above result indicates that this would lead to a fixed added thickness to all of the results of, say, 0.48 nm. However, there could be some wafer-to-wafer variability in this contamination. From our earlier discussion of the repeatability of the XPS data, which for the

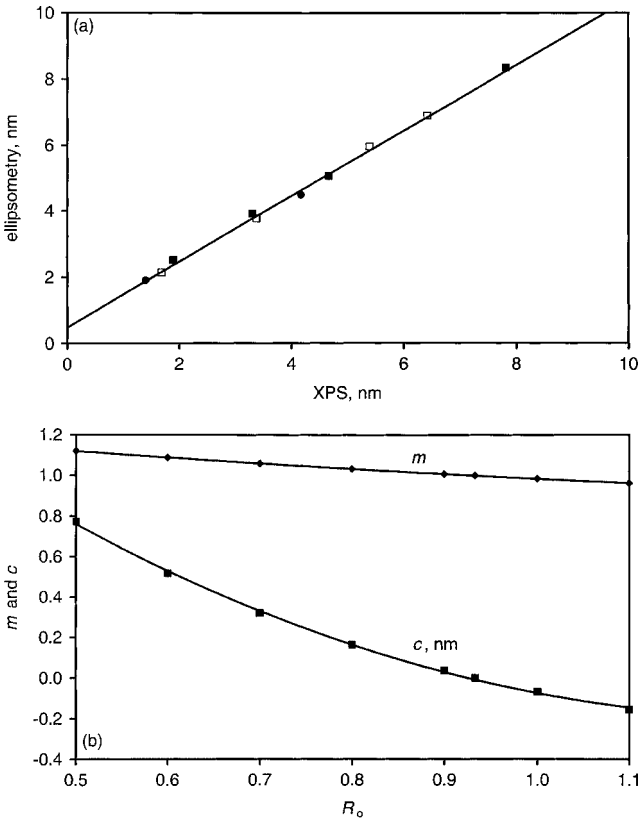

Figure 5. (a) A correlation plot of a set of ellipsometry data from the NPL, with the NPL reference values determined by XPS using the reference geometry and Eqns (2)–(6). The least-squares-fitted straight line gives the gradient m as a scaling constant and the intercept c as an offset value. The rms scatter of the results about the line gives a measure of the combined repeatabilities of the two methods. The European samples are shown for (100) (■) and (111) (□) substrates; (●) the US samples. (b) Variation in m and c values versus R_o for XPS data recalculated from intensities originally correct for $R_o = 0.9329$. Note that these data are for samples soon after preparation and without removal from a dust-free environment between manufacture and ellipsometric measurement.

average of the two sets used here is 0.026 nm, and from the value for r, the contamination variability is <0.085 nm from wafer to wafer. Because the gradient here is 0.993 ± 0.016, the thicknesses of individual samples from a given wafer, which may differ from the samples analysed at NPL using XPS to which they are referred, have reference thicknesses d_{RT} given simply by the sum of the NPL XPS value and the difference in thickness determined by the ellipsometry maps between the individual samples sent out and the samples measured by XPS at NPL. These differences in thickness can be determined to a precision of 0.002 nm. Application, therefore, of the non-unity scaling between these XPS and ellipsometry data will generate a further offset of less <0.002 nm and so may be ignored. The above ellipsometry correction to the reference thicknesses significantly improves the accuracy of the work.

It is useful, before proceeding further, to assess the behaviour of the XPS data arising from variations in the assumed values of R_o and L_{SiO_2}. The effect of L_{SiO_2} is clear. An increase of 1% in L_{SiO_2} for the reference thickness

determinations will simply result in all m values decreasing by 1%. The effect of R_o is more complex, as shown in Fig. 5(b). Here we see how m and c, for XPS intensity data calculated with the R_o value shown on the abscissa, would change for materials whose true thickness was given by $R_o = 0.9329$. Earlier we indicated a standard uncertainty in the R_o value of 2%. If R_o is 2% higher, the m and c values would fall by 0.004 and 0.020 nm, respectively. Therefore, if the d_{RT} values were recalibrated with this higher R_o value, the m and c results from other respondees would rise by these values. At the present time, the uncertainties that we shall deal with in the interlaboratory comparisons are significantly larger than these values. The use of the very low theoretical value of 0.53 for R_o,[20] causes m to rise to 1.108 and c to rise to 0.689 nm but, significantly, causes non-linearity in the plot so that r for perfect data would rise from zero to 0.080 nm.

Note, in Fig. 5(a), that there are three symbols to separate the material from the two manufacturing sources and also the (100) and (111) materials from one of these sources. In this plot there is no significant difference in their behaviours. This is the case for all of the plots and so we assume that, apart from the channelling effects discussed later for the different orientations, there is no significant difference between these materials except for the oxide thickness.

We report the above m, c and r values together with details of the analyses made for each set of results. We also recalculate the data for changes in the input parameters (such as density, etc.) in order to bring all of the results to a common basis. Finally, we consider the XPS data where it is known that the precise R_o values that are applicable depend on the geometry of the analysis. All XPS analysts responding between July and October 2002 were therefore invited to remeasure the data under the reference conditions given earlier.

To provide a perspective, if we analysed Cole *et al.*'s data[14] from Fig. 1 in the above manner the m values would range from 0.8 to 1.7 and the c values from −1.0 to 2.3 nm. We now present the data reported for the different methods in the order given in Table 1.

Medium energy ion scattering

Medium-energy ion scattering is a well-established technique for measuring thin-film quantities. Two laboratories provided MEIS data: the Korean Research Institute of Standards and Science (KRISS) and Daresbury Laboratory. Both used proton beams incident and emitted along channelling directions of the substrate. This reduces the scattering intensity of the substrate. In the recoil of the protons from the target atoms, a collision occurs with energy and momentum given to the target atom. This binary event leads to the scattered protons being detected at a lower energy defined by the target atom mass and the scattering angle. The method is thus analytical and the intensity scattered provides the number of atoms per square metre in the scattering layer. In this way, the amount of oxygen at the surface could be obtained. Additionally, because the silicon atoms in the amorphous oxide are not on low-index crystal directions, the amount of Si also may be obtained. This Si level will include all of the Si in the intermediate oxides together with the Si in the surface layers of the substrate visible to the beam and detector.

In the MEIS experiment, the incident protons slow down in the surface zone at a rate given by the stopping power, dE/dx, both before and after the binary scattering events leading to detection. Instead of measuring the thickness from the scattered intensity, which requires an accurate knowledge of the cross-section, the thickness may be determined from the extent of these losses because dE/dx is known more accurately. The measured range of energy losses, ΔE, is K times the losses on the incident path added to the losses in the emitted path (where K, the kinematic factor, is the ratio of the scattered energy to the incident energy for a given beam ion and target atom). The kinematic factor K depends solely on these relative masses and the scattering geometry. For 125° scattering, for instance, K is 0.8200 for oxygen and 0.8932 for silicon. Thus, ΔE and the film thickness d are related to the angle of incidence of the ion beam, θ_i, and the angle of emission of the scattered ions, θ_o, by

$$d = \frac{\Delta E}{[K(dE/dx)_{in} \sec\theta_i + (dE/dx)_{out} \sec\theta_o]} \quad (8)$$

The accuracy of d depends mainly on the accuracy of measuring ΔE, θ_i and θ_o and the accuracy with which the stopping power, dE/dx, is known. The latter parameter may be calculated or determined experimentally.

In the KRISS study, 100 keV protons were incident along the [111] direction in the (011) plane and the scattered ions were along $[00\bar{1}]$ with a 125° scattering angle. Details of this analysis are given by Chang *et al.*[16] The data given by Chang *et al.* are similar to the present data provided in Fig. 6. The electronic stopping power for 100 keV protons in SiO_2 is tabulated and calculated by Andersen and Ziegler[34] via an empirical equation to be 118 eV nm^{-1}. This value is also given in ICRU Report 49.[35] The change in dE/dx in the energy range 80–100 keV is small[34] and so, in Eqn. (8), the values for $(dE/dx)_{in}$ and $(dE/dx)_{out}$ at 100 keV and 89 keV, respectively, are taken to be equal. Here a value of 122 ± 4 eV nm^{-1} is used, derived from the TEM data from KRISS shown later. The spectra are modelled by taking into account the electronic straggling broadening of 0.1–0.2 keV[36] and the system resolution of 0.4 keV.[37] With this modelling, excellent fits occur with the experimental data. The uncertainties in most parameters are small. The

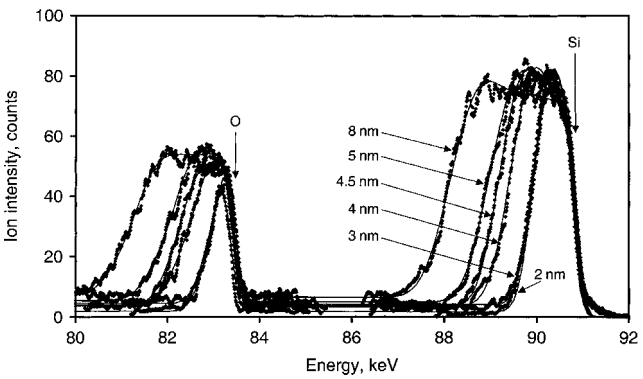

Figure 6. The MEIS spectra with theoretical fits from KRISS for the six oxides on Si(100) using 100 keV protons in the double alignment mode with a scattering angle of 125°.

scattering angle is determined to 0.5°. The most important uncertainty is the measurement of the scattered peak FWHM which leads to an uncertainty of 5% for the thinnest films and <2% for the thicker films. The value of the stopping power has a standard uncertainty of 4.0%. The uncertainty in the path length and geometrical terms is ~1%. Added in quadrature, these gave a standard uncertainty of 6.5%, falling to 4.6% for the thicker films. These uncertainties are type A uncertainties, except for the stopping power which is a type B uncertainty. The results of the fits for the six (100) samples studied with the NPL data (as received) are given in Table 3, along with the values that would be obtained using the SRIM-2003.02[38] stopping power of 120.5 eV nm^{-1} for the incident protons in SiO_2, 121.8 eV nm^{-1} for the protons reflected from Si atoms and 122.2 eV nm^{-1} from O atoms. Also shown in Table 3 are the KRISS values for the Si thickness. The Si thickness should be equal to the SiO_2 thickness plus an added contribution for the initial layers of the Si substrate seen by the ion beam. This added contribution would not be the same for both the (100) and the (111) samples but here only the (100) samples were analysed.

We see from the data for the SiO_2 'monolayer' given in the previous section that a monolayer of water would appear equivalent to 0.25 nm of extra SiO_2. Because MEIS analyses all of the oxygen present, it will sum all of the oxygen in the SiO_2 and add any oxygen in adsorbed water layers or oxygen in the carbonaceous contamination. At least one monolayer of chemisorbed water is expected to remain on the SiO_2 surface *in vacuo*. Thus, in obtaining the fit against the NPL data we expect an offset value of c in the range 0.25–0.50 nm to arise from these oxygen-containing contaminations contributing to the MEIS data. The non-unity value of m arises from the uncertainties in the dE/dx value here and in the L_{SiO_2} value used for the XPS data. The agreement between the m values for the oxygen and the silicon confirms the stoichiometry of SiO_2 to within 6%. This supports the earlier result of a correct stoichiometry to 1.6 ± 2.1% by XPS.[20] The difference in the offset c values between the silicon and oxygen data of 0.956 nm is approximately in line with the earlier study of Chang *et al*.[16] where a value of 1.08 ± 0.22 nm may be calculated. The Si data are expected to include between one and two monolayers of the Si substrate, equivalent to 0.62–1.23 nm of SiO_2.

In the Daresbury Laboratory study a 102.8 keV proton beam was used, incident along the $[\bar{2}1\bar{1}]$ direction for the (100) samples and along $[\bar{1}\bar{1}0]$ for the (111) samples. Here a scattering angle of 90° was chosen to detect the emitted ions along the [111] and [001] directions, respectively. The analysis here is similar to that from KRISS. An energy-dependent stopping power from the latest version of SRIM (SRIM-2003)[38] is used in the fitting procedure. This fitting procedure recently has been employed successfully in measuring the thicknesses of ultrathin oxides on 4H-SiC.[39] This stopping power changes by ~0.1% over the relevant energy range. In addition to the data provided by KRISS, seven repeats of the 5 nm (100) sample were made. Correlation with the NPL data using XPS is given in Table 3. In the use of the SRIM code, if the SiO_2 density is reduced from the SRIM default value of 2.32 g cm^{-3} to 2.196 g cm^{-3}, the stopping power for 102.8 keV protons reduces to 120.09 eV nm^{-1} and the thicknesses increase. For consistency, we provide these data for the latest SRIM-2003 stopping powers also in Table 3. Again, the m values for oxygen and silicon are similar and the offset for Si is ~0.8 nm higher than for oxygen. The result for m appears to be 3.9% greater than the equivalent result from KRISS. This differences exceeds the precision of the data because, as we shall show later, the typical uncertainty of 0.13 nm in each result leads to an uncertainty of ~2.4% in the gradient m. The reason for this difference is not clear because the main source of error, the value of dE/dx, is removed in the comparison.

In Table 3 there are two sets of values. The first set is the data as supplied but these data for KRISS depend on traceability via TEM that is entered separately in the TEM

Table 3. The MEIS results

Laboratory	m	c (nm)	r (nm)	Repeatability of 5 nm (nm)	dE/dx (eV nm^{-1})
KRISS (O)[a]	0.892	0.553	0.100	—	122
KRISS (O)[b]	0.903	0.559	0.102	—	SRIM 2003, 120.50
KRISS (Si)[a]	0.954	1.478[c]	0.153	—	122
KRISS (Si)[b]	0.966	1.496[c]	0.155	—	SRIM 2003, 120.50
Daresbury Laboratory (O)[a]	0.892	0.385	0.145	0.132	126.87
Daresbury Laboratory (O)[b]	0.942	0.406	0.153	0.139	120.09
Daresbury Laboratory (Si)[a]	0.946	1.031[c]	0.136	0.192	126.87
Daresbury Laboratory (Si)[b]	0.999	1.089[c]	0.144	0.202	120.09
Average[a]	0.921	0.469[d]	0.134		122, 126.87
SD[a]	0.033	0.119[d]			122, 126.87
Average[b]	0.953	0.482[d]	0.138		120.50, 120.09
SD[b]	0.040	0.108[d]			120.50, 120.09

[a] Results originally supplied.

[b] Homogenized data using an SiO_2 density of 2.196 g cm^{-3}

[c] Offset for Si is not related to the offset for O, as discussed in the section on MEIS.

[d] Excludes Si offsets.

section for KRISS. The second set uses values of dE/dx from SRIM-2003, consistent with the common SiO_2 density of 2.196 g cm^{-3}, to provide comparison. Although we quote the thickness here in nanometres it is clear that we actually measure atoms m^{-2} because, if the value of the density is increased, the stopping power increases and the deduced thickness in nanometres falls. Thus, the quoted thickness in nanometres is density dependent but the thickness in atoms m^{-2} is not.

Nuclear reaction analysis

Nuclear reaction analysis, like MEIS, allows the total oxygen content in a film to be evaluated. In this method, a deuteron beam is used to strike ^{16}O atoms and protons are detected from the $^{16}O(d,p_1)^{17}O^*$ reaction. This method has been in use for many years by the Groupe de Physique des Solides at the University of Paris to calibrate the oxygen contents of films.[40–42] Figure 7 shows the dependence of the cross-section for this reaction on the deuteron beam energy. A beam energy of 860 ± 10 keV is selected to be on the flattest part of the plateau in order to remove any cross-section changes that would occur as the beam penetrates the film and slows down. This is not a concern for the thicknesses studied here but the method is also set up to measure much thicker films.

In order to make this method quantitative, one either needs the absolute cross-sections and detector solid angles or one inserts a sample with a known number of oxygen atoms per square metre as a calibrant. Quantities are then derived from the counting ratios for the reference and the film to be measured. These are linear up to and beyond film thicknesses of 100 nm. Here, as a calibrant, a reference sample of Ta_2O_5 was made with (678 ± 21) × 10^{19} atoms m^{-2} using oxygen of natural isotopic composition by anodic oxidation. This value was obtained by comparison, in turn, with a primary reference sample. By measuring the surface area of the tantalum foil and by measuring the charge transfer by coulometry, the number of added oxygen atoms per square metre in the primary reference sample was determined. The uncertainty in this primary reference sample was the dominant uncertainty. The above thickness is approximately equivalent to 126 ± 4 nm and the uncertainties cover any prior adventitious oxide. Errors in the coulometry may arise if there are currents passed that do not lead to an oxide deposit. This needs extreme care with materials and sample preparation, as detailed by Amsel *et al*.[40–42] and by Pringle[43] and Seah *et al*.[44] This was done here.

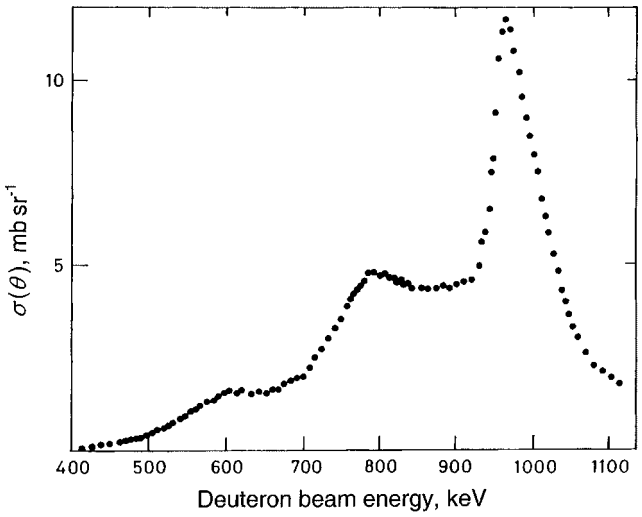

Figure 7. Oxygen cross-section in NRA as a function of the deuteron beam energy, after Amsel and Samuel.[40].

The results from the University of Paris are shown in Table 4. The uncertainties arise from the reference sample (3.1%), the assumed SiO_2 density of 2.21 g cm^{-3}, the counting statistics and the baseline subtraction method. The uncertainty in the counting statistics for the 5 nm sample leads to the rms scatter of 0.153 nm. The uncertainty in the SiO_2 density is considered by re-deriving the data, as shown in Table 4 for the consistent density of 2.196 g cm^{-3}. The uncertainty in the NRA calibration sample leads directly to a standard uncertainty of ±0.031 in the gradient m, in addition to the fitting uncertainty of 0.013 in the gradient. Thus, the gradient m for the consistent density traceable to the quantity of charge is 1.074 ± 0.034 at one standard deviation. The offset of 0.480 nm is similar to the offsets seen in MEIS and arises from the oxygen for the same reason as given there. In view of the significantly higher m value found here, in subsequent work in Paris, the data were checked against an earlier secondary Ta_2O_5 reference fabricated at 80 V and three further Ta_2O_5 primary references fabricated at 140 V and 280 V. These results were all consistent with each other, reaffirming the m value of 1.074 ± 0.034.

Rutherford backscattering spectrometry

Rutherford backscattering spectrometry has many of the attributes of MEIS but works at higher beam energies. This allows thicker films to be measured for total quantity as in NRA but the poor energy resolution does not permit the thickness to be measured using the stopping power and energy spectra. Instead, the total peak intensities are used. In RBS the cross-sections may be calculated with great accuracy from the Coulomb potential, but at higher beam energies the cross-sections have non-Rutherford isotope-specific resonances. In particular, the elastic non-Rutherford backscattering (EBS) $^{16}O(\alpha,\alpha)^{16}O$ resonance at 3036 keV with

Table 4. The NRA results

Laboratory	m	c (nm)	r (nm)	Repeatability (nm)	SiO_2 density (g cm^{-3})
University of Paris[a]	1.067	0.477	0.153	0.198	2.21
University of Paris	1.074	0.480	0.154	0.199	2.196

[a] Results originally supplied.

a ^{4}He beam was used by two participants. This EBS mode gives an enhancement of a factor of 20 to the Rutherford cross-section for oxygen but it is necessary to determine the beam energy very precisely. The RBS studies have been completed in The Netherlands and Singapore, whereas EBS studies have been completed in Germany and the UK.

In the Centre for Ion Beam Applications at the National University of Singapore (NUS), RBS spectra are measured using a single-alignment channelling mode with normal incidence that reduces the Si signal background that would lie under the oxygen signal. Channelling greatly improves the signal-to-noise ratio for the oxygen signal. In this work a 2 MeV He^+ ion beam is used and the detected ions are monitored at 112.5° scattering angle using the IBM geometry. The oxygen signal, Y, is then related to the thickness, d, via the equation

$$Y = Nd\sigma\Omega Q \quad (9)$$

where N is the oxygen atomic density (4.402×10^{28} atoms m^{-3}), σ is the cross-section, Ω is the detector solid angle and Q is the integrated charge from the beam. In this work, the charge measurement was not done with these samples because emitted secondary electrons would cause small errors. Instead the current was normalized by monitoring both before and after analysing each sample, using a WSi sample from Semiconductor Manufacturing. This sample was characterized to have a $WSi_{2.6}$ layer with 8.3×10^{17} atoms cm^{-2} on top of SiO_2 with 3.5×10^{18} atoms cm^{-2} in turn on an Si wafer. The total beam doses were then determined from the WSi sample using the SIMNRA stopping powers and internal charge normalization (using the Si in the substrate). The system is intensity stable but this was done to ensure optimum accuracy. The solid angle, Ω, of 3.35 msr was determined from direct geometrical measurement. The Rutherford cross-sections are analytical and here the value was 162.9 mb sr^{-1},[45] with a screening correction of 0.2%,[46] using the SIMNRA code.[47] These accuracy values are discussed by, for instance, Wätjen and Bax,[48] where they estimate the uncertainty for Bi as 0.5% for a screening correction of 0.978 and where the screening correction for a 2 MeV beam of He in Si is 0.998.

The results for the fits for the NUS data to the NPL data for the oxygen peak are shown in Table 5. The rather high scatter arises from the low intensity of the peak. The statistics of the counts in the oxygen peak lead directly to a standard uncertainty of 0.29 nm. The offset c arises for the same reasons as given for MEIS and NRA and is consistent with those figures. The gradient m is 1.072 ± 0.032 from the statistics of the fit to the NPL thickness data. Note that here, again, it is Nd (oxygen atoms m^{-2}) that is being measured.

In addition to the oxygen data, Si thicknesses may be evaluated from the NUS measurements as shown in Table 5. This was conducted in two separate runs of a full and a partial set that gave different offsets. Here the offset is more critically dependent on the accuracy of the alignment settings and this may be different between the two runs. As for MEIS, the Si offset is higher than for the oxygen because the beam sees the first layers of the substrate. The important parameter here is the gradient, which for the two runs for Si averaged 0.927.

Table 5. The RBS and EBS results

Laboratory	m	c (nm)	r (nm)	Repeatability between runs (nm)
NUS (O)[a,b]	1.072	0.351	0.510	0.524
NUS (Si)[a,b]	0.927	4.643	0.359	0.866
Philips (O)[a]	0.919	0.481	0.271	—
Philips (O)[b]	0.968	0.506	0.286	—
University of Jena (O)[a,b]	0.981	0.463	0.253	0.192
University of Surrey (O)[a,b]	1.075	0.950	0.168	—
University of Surrey (Si)[a,b]	1.063	7.023	0.431	—
Average[a]	1.006	0.561[c]	0.332	
SD[a]	0.073	0.266[c]		
Average[c]	1.014	0.568[c]	0.334	
SD[c]	0.064	0.263[c]		

[a] Results originally supplied.
[b] Homogenized data with SiO_2 density of 2.196 g cm^{-3}.
[c] Excludes Si offsets.

Studies were also conducted at Philips but, owing to a shortage of samples, the samples already studied at Philips by XPS were re-used as described at the end of the section on XPS. Rutherford backscattering spectrometry was conducted with a 2 MeV He^+ ion beam, with ⟨100⟩ or ⟨111⟩ alignment channelling conditions normal to the surface to reduce the substrate background signal and an 86.5° scattering angle. The results were similar to those of the NUS and it was estimated that some uncertainty arose from the need to remove the background under the peak using a third-order polynomial. Calculations were made using Eqn. (9) in the surface approximation, where the cross-sections are constant through the layer, with $\sigma(O) = 0.284 \times 10^{-24}$ cm^2 sr^{-1}, $\sigma(Si) = 0.892 \times 10^{-24}$ cm^2 sr^{-1} and Ω ~0.57 msr. Some uncertainty arose in the measurement of the integrated charge arising from the state of the SiO_2 surface and so this was normalized by using the Si surface peak.[49] Here the content for the Si peak is set to be half the amount of the oxygen plus, for ⟨100⟩, 15.5×10^{15} Si atoms cm^{-2} and, for ⟨111⟩, 13.5×10^{15} atoms cm^{-2}. Rutherford cross-sections are available in the handbooks by Ziegler[50] and also by Tesmer and Nastasi,[45] but here the cross-sections are derived using the RUMP programme[51–53] because experience in Philips has found good consistency with ellipsometry, step height determinations, inductively coupled plasma optical emission spectroscopy, electron microprobe and x-ray fluorescence in different situations The density of the SiO_2 was taken as 6.96×10^{28} atoms m^{-3} (2.315 g cm^{-3}). Results for the oxygen thickness were fitted to the NPL data to give the m, c and r values, as shown in Table 5. These data were then scaled to the common density of 2.196 g cm^{-3} to give the new m, c and r values also listed in Table 5. The RBS spectra for these samples showed 0.8–10% of a monolayer of a heavy metal contamination at the surface, not seen elsewhere and assumed to arise from the prior study by XPS. This contamination, identified as barium by SIMS, will not affect the results from RBS.

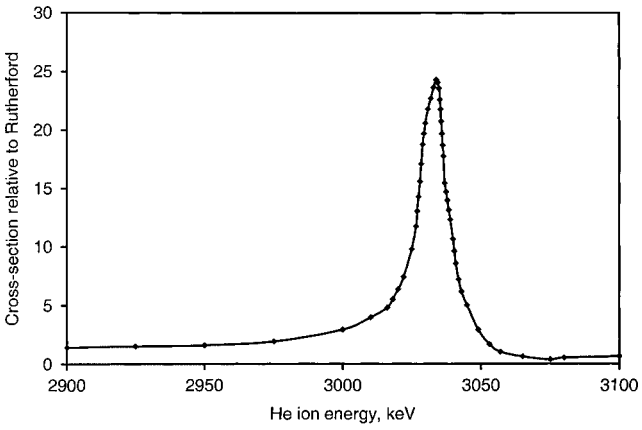

Figure 8. Ratio of oxygen scattering cross-section relative to Rutherford as a function of the He^+ ion energy, as fitted at the University of Surrey to 0.99 times the data of Cheng *et al*.[55].

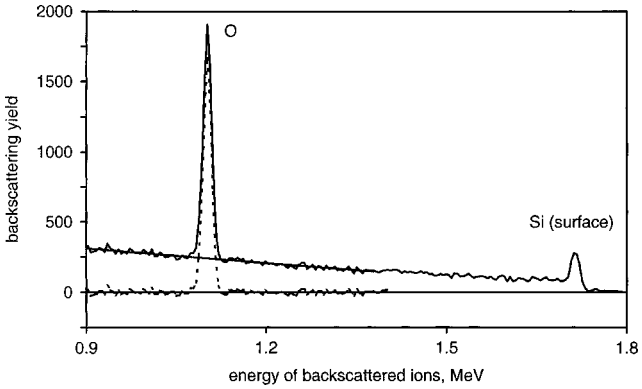

Figure 9. Rutherford backscattering spectroscopy analysis of the 5 nm oxide on Si(100) using the enhanced cross-section at 3.036 MeV for He^+ at the University of Jena and the channelling condition to reduce the Si background. The inclined straight line shows the linear background to define the peak area and this is subtracted to show the oxygen peak area. Note the excellent signal-to-noise ratio.

Extensive EBS studies were conducted at the University of Jena using 3036 keV He^+ ions, again using the normally incident channelling geometry with a scattering angle of 168°. This beam energy was chosen because it is on the peak of the enhancement above the Rutherford theoretical value,[54,55] as shown in Fig. 8. The beam energy was established by altering potentials to maximize the oxygen signal. Calculations showed that overlayers of carbonaceous contamination far in excess of those found here would be needed to affect the maximum significantly. A typical spectrum showing the enhanced signal quality is given in Fig. 9. The cross-section was determined by fitting a bulk SiO_2 spectrum, assuming TRIM85 stopping powers for O[56] and stopping powers for Si[57] The amount of scattering depends on the cross-section but the height of the spectrum, i.e. the intensity per unit energy loss, depends on the stopping power. The issues concerning accuracy are discussed by Jeynes *et al*.[58] Compared with the stopping power of SiO_2[59] used in the following work at the University of Surrey, this procedure underestimates the oxygen content in the thin surface films by 6%.

For calculating the thickness, because the ions are at normal incidence, Eqn. (9) is used again. The sources of error are estimated from experimental measurements as follows. The integrated charge has an error arising from inadequacy of the suppression of secondary electron emission. Here tests indicate an uncertainty of 1%. The solid angle of the detector for three determinations shows a scatter of 0.25% but the real uncertainty arises from the setting of the beam energy to the peak of the cross-section. These lead to an unknown uncertainty. Repeated results for the 5 nm sample, one after the other, show a short-term repeatability standard deviation of 0.118 nm but repeated results for the set, over a longer interval, indicate a repeatability of 0.192 nm. Using the average of two separate sets of data, the fit with the NPL result using a density of 2.196 g cm^{-3} for SiO_2 gives the values indicated in Table 5. Again, we see a gradient m close to unity and an offset consistent with the other oxygen data. In this case, the enhanced intensity of the oxygen peak has improved very significantly both the repeatability and the rms scatter shown in Table 5.

A similar approach is taken in the University of Surrey Ion Beam Centre using the elastic non-Rutherford backscattering $^{16}O(\alpha,\alpha)^{16}O$ resonance at 3036 keV with a $^4He^+$ beam, the detector at 167° and a normally incident ion beam (within 0.5°) for channelling analytical geometry. Careful measurements of the cross-section have been made by Cheng *et al*.,[55] showing 20 times the Rutherford cross-section for 170° scattering, and by Feng *et al*.,[60,61] showing 14 times the Rutherford cross-section at 165°. Here Cheng *et al*.'s data are used because the change with energy, measured here, fits Cheng *et al*.'s data better than those of Feng *et al*. Three measurements were made for each sample except the 5 nm (100) sample for which ten measurements were made. Extra measurements were made for a certified reference material (CRM) with a certified Sb layer[62] and a thick SiO_2 sample to measure the detection solid angle and other data, as well as checking Cheng *et al*.'s cross-section (which is at a 3° greater scattering angle). To do this, the energy loss, dE/dx, in SiO_2 is needed and here we use a linear combination of the Si energy loss given by Barradas *et al*.,[57] the energy loss in SiO_2 as given by Pascual-Izarra *et al*.[59] and parameterized by Boudreault *et al*.[63] and the energy loss for Sb given in the TRIM85 compilation[56] to fit the spectrum carefully. We should note that these values for the energy loss in SiO_2 are supported by recent measurements by Lennard *et al*.,[64] as discussed in Reference 63. These terms lead to a total uncertainty of 5–8% in the effective cross-section σ used here, arising from 2% in the SiO_2 stopping power, 2% in the oxide layer thickness of the IRMM CRM, 3% for the resonance curve shape and 3–7% from the sensitivity of the oxygen yield to the beam energy uncertainty (the beam energy uncertainty is <500 eV or 0.017% but it drifted by 3 keV or 0.1% during the analysis). The resulting cross-section is 1% lower than that of Cheng *et al*. and so the latter's data (with interpolation points) are used with a multiplier of 0.99, as shown in Fig. 9.

The combined uncertainty in $Q\Omega$ is 2.6% coming from type A estimates of 2% for Q, 1.5% for counting statistics and 0.6% uncertainty in the CRM. Counting statistics for the thin oxide films were between 1.2% and 4.5% for the O signals

and 2.8% and 7% for the Si signals. Thus the combined standard uncertainty for the O signals, which mainly arises from the type B uncertainty of the cross-section, is ~6% for most of the samples and rising to ~10% for the last sample to be measured. The combined standard uncertainty for the Si signals, which arises from type A uncertainty (because the cross-section for Si scattering is Rutherford and is known very accurately), varies between 3.8% and 7.5%. The fit of the data to the NPL measurements gives m and c as given in Table 5.

In this work the spectrum is fitted using the 'DataFurnace' simulated annealing code[65,66] and a model of an oxide layer, an amorphous Si interfacial layer and a crystalline Si substrate. In the model, the Si signal comes from the Si atoms in the amorphous oxide as well as the first few atomic layers of the crystalline substrate, so any extra Si signal comes from this interlayer. Using this model, the Si-channelled substrate background to the Si surface peak is accurately fitted in the model. These data are all calculated in atoms m^{-2} and are converted to nanometres using a density for thermal SiO_2 of 2.196 g cm^{-3}.

The data here give this interlayer thickness as 2.655 ± 0.179 nm for the (100) samples and 2.110 ± 0.288 nm for the (111) samples. These uncertainties are the standard deviations for the six and four samples, respectively. We expect the interlayer thicknesses for the (100) and (111) surfaces to differ but to be constant within each orientation. Evaluating the equivalent SiO_2 thickness of this interlayer as if the Si atoms were in SiO_2, the thicknesses would all be increased by these values scaled by 2.269 to account for the Si atomic densities in Si and SiO_2. In this way, the offsets c would increase to 7.023 ± 0.406 and 5.786 ± 0.653 nm for (100) and (111) surfaces, respectively. The fits of the data to the NPL measurements give the m and c values for the oxygen and silicon peaks as in Table 5. The m values for O and Si are not significantly different.

This is the last of the data for methods specifically analysing the oxygen content. The average offsets of the oxygen data reported for MEIS, NRA and RBS/EBS are 0.469, 0.477 and 0.561 nm, respectively, averaging 0.502 ± 0.051 nm where the uncertainty is given as the standard deviation of the three methods. The equivalent values using the SiO_2 density of 2.196 g cm^{-3} are 0.483, 0.480 and 0.568 nm, respectively, averaging 0.510 ± 0.050 nm.

Secondary ion mass spectrometry

Secondary ion mass spectrometry was included in this study, not because it was expected to yield highly traceable results but rather to define what it could achieve, bearing in mind its use in profiling thin gate oxides that are not pure SiO_2 but have a nitrogen profile within the oxide. It is a popular method for observing small changes in the nitrogen profile rapidly and economically[67] and for this reason only one set of SIMS data were included with work from Cascade Scientific.

In this work, the samples are profiled using a sputtering beam and the time to the interface is compared with the time to the interface of a thicker layer. To obtain good depth resolutions, the profiling beam energy is reduced to the minimum and a SIMS instrument without a significant extraction field must be used. Thus, a 600 eV Cs^+ ion beam was used in a Physical Electronics Adept 1010 quadrupole mass spectrometer system, with the beam set at 60° to the surface normal. For the profiles, the oxygen concentration is defined by the ratio of the intensities of $^{149}CsO^+$ to $^{161}CsSi^+$. These ions, rather than the higher intensity negative secondary ions, are chosen because they have a much reduced matrix effect between SiO_2 and Si.[67] The ratio is used to correct for any changes in the beam current or detection system. The plateau of the profile is then set to an intensity of 66.7% and the interface is taken as the point when this normalized intensity has fallen to 33.3%, as shown in Fig. 10(a). The fits of the experimental data to the NPL values given in Fig. 10(b) provide the m, c and r values given in Table 6. The depth scale here has been defined by a 10 nm sample with the thickness evaluated by a TEM analysis outside this study.

Note, in Table 6, that this is the first result with a negative offset. This occurs as the initial sputtering depletes the surface

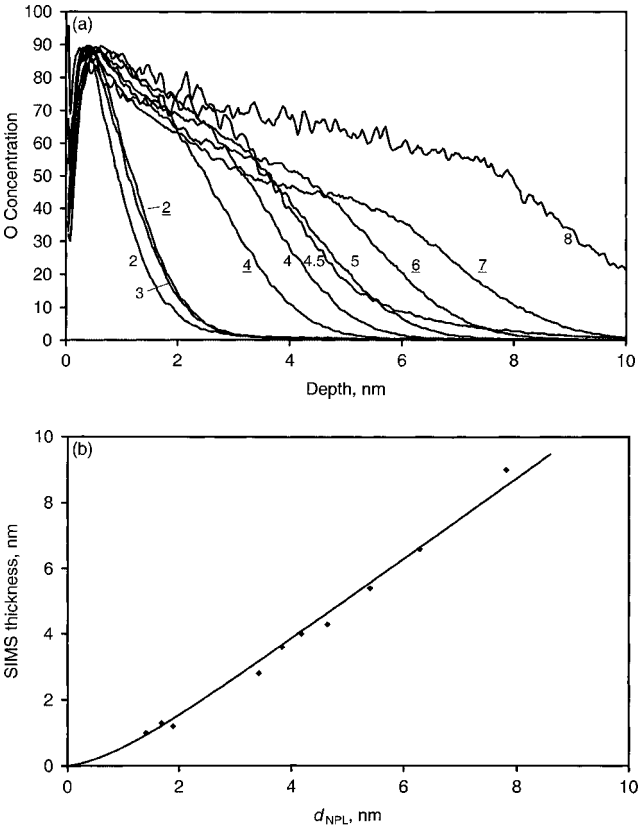

Figure 10. The SIMS data from Cascade Scientific. (a) Profiles for the ten samples with the nominal thicknesses in nanometres; those for the (111) surfaces are underlined (the data have a three point average smooth for presentational purposes. (b) Correlation with the NPL thicknesses.

Table 6. The SIMS results

Laboratory	m	c (nm)	r (nm)
Cascade Scientific[a]	1.227	−1.056	0.260

[a] Results originally supplied.

of oxygen so that the signal level rises to a peak as the contamination falls and then drops again within the first 1 nm. In this first stage we have the 'correct' sputtering rate for SiO_2. After the depletion, the sputtering rate falls because the easily sputtered oxygen is partly removed. Thus, the average sputtering rate falls as the layer thickness rises. This behaviour leads directly to a negative offset. In Fig. 10(b) we fit a straight line as with the other data but at the start is an added contribution of $-c\exp(-d/d_o)$ where the decay constant, d_o, is 1 nm. This fit indicates that the initial sputtering rate could be twice that for greater depths but that the excess speed decays very rapidly. Similar transients over this region have been observed using oxygen sputtering in Si by Wittmaack.[68]

X-ray photoelectron spectroscopy

Studies in XPS may be conducted in a number of ways. The method described at the start of the Results section is the method favoured at NPL in which the spectra are recorded at high energy resolution for one emission angle. If the spectra are recorded using unmonochromated x-rays, the x-ray satellites should be removed first. Analysts do not always use x-ray satellite subtraction and this does lead to small, but significant, errors.[6] Next the spin-orbit splitting of the Si 2p peak, with 50% of the intensity for the $2p_{1/2}$ peak at 0.6 eV higher binding energy[30] than the $2p_{3/2}$ peak, is removed by a deconvolution routine. Spin-orbit subtraction is not always conducted by all analysts. Next, a Shirley background[32] is removed. Some analysts use other backgrounds. Finally, the peak structure may be analysed into the five peaks (5P) described earlier. Some analysts use two peaks (2P). Some analysts do not have the spin-orbit software and so fit the elemental peak with two peaks and the oxide peak with one peak (3P). These different approaches all lead to small variations discussed in detail elsewhere.[6] If only two or three peaks are available, Eqn. (1) is generally used. One then needs the values of L and R_o and, although values are given above, different analysts use different values. In particular, R_o may be calculated from first principles to be 0.53 for either Mg or Al x-rays.[20] This is a factor of 1.76 lower than the measured value reported above[6] and arises from issues concerning the way the peak areas are measured, from uncertainties in some of the input parameters[20] and possible inadequacies of the calculation[69,70] of R_o. Experimental values of R_o range from 0.62 to 0.94,[20] arising from variations in the sample surface condition and the method of interpreting the data.[6]

Even more important than the above effects are the effects of the measurement geometry. If a low index direction such as normal emission is used, it is found that, for thin films, the substrate forward focusing will reduce R_{SiO_2} by a factor, F, of ~1.3 if poor angular resolution is used. However, if high angular resolution is used, F can be significantly greater.[20]. We know that the angular intensity variations in XPS become reduced the further the substrate electrons are transported and scattered through the overlayer. Thus, we may expect the enhancement to decay exponentially to 1.0 with a characteristic length A. In this case we may write, in the formalisms used earlier[20]

$$I_{SiO_2} = I^{\infty}_{SiO_2}\{1 - \exp[-d_{SiO_2}/(L_{SiO_2}\cos\theta)]\} \quad (10)$$

$$I_{Si} = I^{\infty}_{Si}\exp[-d_{SiO_2}/(L_{SiO_2}\cos\theta)]\{(F-1) \times \exp[-d_{SiO_2}/(A\cos\theta)] + 1\} \quad (11)$$

Figure 11(a) shows the thickness that would be calculated if A is ignored versus the true d for an F value of 1.3 and $A = 1.4L$. The data may be fitted by a straight line in the range 1.8–8 nm, which has a negative intercept. Figure 11(b) shows how this intercept value varies in the range zero to −0.25 nm with A/L. The values of F and A, and hence the details of these plots, depend on the low index direction and the solid angle of acceptance of the spectrometer. For these reasons, detection along crystal directions is not recommended because both m and c will exhibit unquantified type B uncertainties. The NPL has derived a reference geometry well away from the low index directions in which Eqns (2)–(6) are valid and are linear to ±0.025 nm.[6] The recommendations to use this reference geometry were published in the middle of the time for response in this interlaboratory study and, by that time, many laboratories had reported their first set of data. All XPS laboratories responding with data by the late Autumn of 2002 were then invited to provide additional analyses at the reference geometry.

Instead of deducing d from Eqn. (1) or Eqns (2)–(6), by using one emission angle θ, some analysts fit a straight line to a plot of $\ln(1 + R_{expt}/R_o)$ versus $\sec\theta$. For $\theta > 60°$, deviations from the above equations occur as a result of the effects of elastic scattering. However, for $\theta \leq 60°$ good

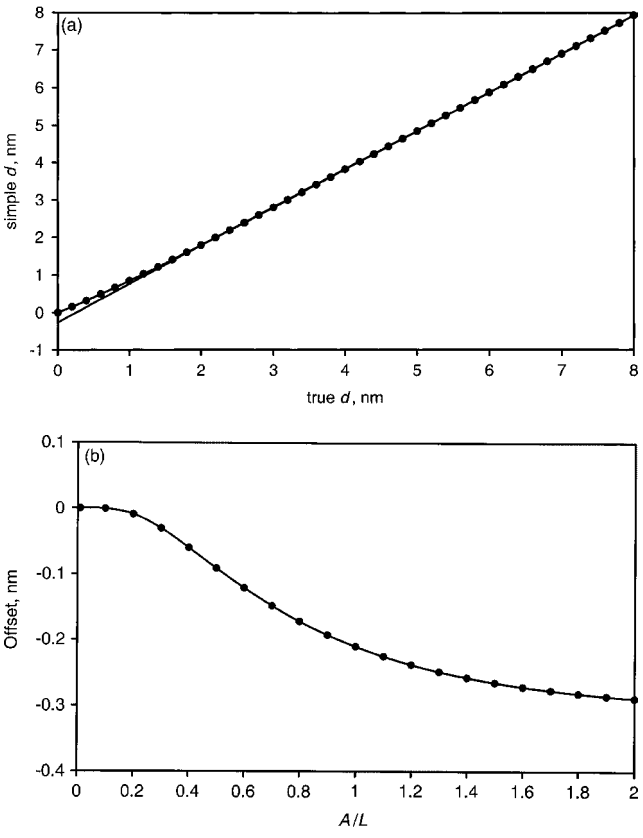

Figure 11. Thicknesses evaluated using Eqn. (1) for data acquired in a low-index direction with an initial substrate enhancement F of 1.3: (a) example of a calibration plot with $F = 1.3$ and $A = 1.4L$; (b) offsets arising for various values of A/L.

results should be obtained in amorphous systems. In this relation, the gradient of the plot gives $d/(L\cos\theta)$ and so d may be obtained. Unfortunately, the effects of forward focusing from the substrate lead to a slight offset in the line for this plot so that, instead of fitting to a straight line through the origin, there is a negative offset so that the gradient and hence d become erroneously increased. This occurs most strongly for the thinnest oxides where the forward focusing is strongest and so we would expect this approach to lead to a fit against the NPL data that gives rise this time to an erroneous, positive offset c. Additionally, the greater degree of uncertainty of the $\ln(1 + R_{expt}/R_o)$ versus $\sec\theta$ plot leads to a greater uncertainty in the determination of d in addition to the above bias.[26] If data are recorded at many angles, the most accurate procedure is to use the average of the thickness data for $\theta \leq 60^\circ$, including angles that avoid low-index crystal directions. The effects of forward focusing in the deduced value of d as a function of emission direction are shown clearly in Refs 20 and 26.

The above methods are the traditional methods for XPS. In recent years a different method has been developed to measure quantities as a function of depth, which has been tested here. This method concerned the contributions to the background shape in spectra, following the XPS peaks, that arise from transport through the solid.[17,18] For a monolayer of oxygen, the background behind the peak is at almost the same intensity as that at energies higher than the peak. As the layer thickness increases, the extra background at lower kinetic energy than the peak increases with respect to the peak intensity and extends to lower energies. In this method, the loss spectrum is removed from the peak for various trial models of the depth profile until the background is removed correctly. The shape and intensity of the corrected spectrum are compared to those of a reference of a bulk SiO_2 sample (an oxide thicker than 15 nm) after background removal using a Tougaard Universal three-parameter inelastic scattering cross-section. In this way the film thickness is deduced with the main uncertainty deriving from the attenuation length L that appears in Eqns (1)–(6), except that here it is the L value at the energy of the O 1s peak rather than for the Si 2p peak. This method is known as the extended O 1s peak with QUASES-Tougaard.[19] The calculations are not simple but mainly rely on the precision of the correct background subtraction (3–5%) and the accuracy of the attenuation length (17.4%[3]). In a second method[71] that involves minimal operator interaction, a very simple algorithm automatically takes the XPS background effect into account and this method is also tested here. This 'AOS in 3λ' algorithm is less accurate but well suited for automation and gives the amount of atoms within the outermost ~3λ. These methods are important for evaluating profiles of composition through films, rather than evaluating the single parameter d. They could be used, like SIMS, for analysing the distribution of the nitrogen in oxynitride films.

We consider first the results from the Bundesanstalt für Materialforschung und prüfung (BAM). Here, a Surface Science Industries SSX-100 instrument was used with a focused, monochromated Al x-ray source. The photoelectron emission was measured at 0° emission angle and the thickness was calculated via Eqn. (1) by analysing the Si 2p elemental and SiO_2 peak intensities after removal of a Shirley background. In this case, three peaks were analysed, the elemental peak being a spin-orbit pair without fixing the energy shift or relative intensities. The thicknesses, d, were calculated from Eqn. (1) using a calculated value of $R_o = 0.531$. The value of L_{SiO_2} (Al) was taken to be 0.92 times[72] the IMFP that is given by Tanuma, Powell and Penn.[33] The m, c and r values from the fit of the results reported with the NPL thickness data are given in Table 7. In this work, the uncertainties were estimated as 20% for the IMFP (which dominates the systematic contributions) and 20% from R_{expt}. From the results in Table 7, we see that the repeatability is indeed very good but we note that the value of R_o is very much less than that determined experimentally. If the values of L_{SiO_2} and R_o listed earlier are used, the m value approaches closer to unity and the offset c reduces as shown in Table 8. The thinnest sample has reduced by 0.751 nm from 2.095 nm, and the thickest by 1.901 nm from 10.243 nm. The observed negative offset was predicted for this geometry with emission along the [100] direction, as in Fig. 11(b). From this we deduce $A/L = 0.53$ or $A = 1.8$ nm. This value of A tells us how rapidly the elastic scattering in SiO_2 removes the forward focusing from the Si substrate. Depending on the entrance angle of the spectrometer, this will happen at some small fraction of the transport mean free path length because only 15° or so of angular scattering is required. Using the NPL reference geometry in this instrument led to a scaling factor closer to unity but a higher offset, as shown by the entry for BAM (RG) in Table 7. However, using the NPL values for L and R_o in Table 8 we now see that the scatter has halved, the scaling factor is within 1% of unity and the offset is less than the measurement repeatability. This remarkable result shows the improvements possible by using the reference geometry and consistent R_o and L values.

Next, we consider the data from the Nanostructured Material Group, National Research Council of Canada (NRC), that were made using a Kratos Axis Ultra instrument with a monochromated Al x-ray source. The photoelectron emission was measured for 0°, 10°, 20°, 30°, 40°, 50°, 60°, 70°, 75°, 80° and 85° emission angles from the surface normal and the thicknesses were calculated using two peaks and Eqn. (1). To fit the two peaks, a single straight-line background was used for about half of the samples but for the thinner samples a simple baseline involving an 'over-smoothed' algorithm was used. As noted in a previous work,[6] the straight-line background will lead to an overestimate of the thickness for the thicker samples. The 'over-smoothed' method removes areas from both peaks and the result may be an over- or underestimate of thickness. The value of R_o was determined by lightly sputtering a 40 nm oxide sample to obtain $I^\infty_{SiO_2}$ and then fully removing the oxide to measure I^∞_{Si}. The value of R_o as an average of two determinations was 0.91 but it should be noted that this may involve some reduction of the $I^\infty_{SiO_2}$ value as a result of preferential sputtering. Another value for R_o of 0.6 was also used[14,73] as the lowest measured published value but was later rejected. The value of the attenuation length L_{SiO_2} was taken as 3.47 nm from the data of Powell and Jablonski.[72]

Table 7. The XPS results originally reported

Laboratory[a]	No. of peaks	m	c (nm)	r (nm)	Repeatability (nm)	L_{SiO_2} (nm)	R_o
BAM	2	1.248	0.429	0.094	0.055	(Al)3.47	0.531
BAM (RG)	2	1.135	0.741	0.096	0.028	(Al)3.47	0.531
NRC	2	0.959	−0.143	0.123	0.175	(Al)3.47	0.91
NRC (RG)	2	0.998	−0.147	0.092	—	(Al)3.47	0.91
NMIJ	2	1.060	−0.244	0.081	0.075	(Al)3.39	0.70
University of Utsunomiya	2	1.209	0.957	0.187	0.197	(Al)3.77	0.525
University of Utsunomiya	2	1.101	0.244	0.162	0.198	(Al)3.77	0.87558
University of Utsunomiya (RG)	2	1.268	0.867	0.094	—	(Al)3.77	0.525
University of Utsunomiya (RG)	2	1.143	0.122	0.086	—	(Al)3.77	0.87558
NTT	2	1.236	−0.234	0.171	0.080	(Al)3.77	0.8278
NIMS	2	1.075	0.043	0.135	0.041	(Mg)3.07	0.6803
PSB	2	0.871	0.228	0.076	—	(Al)2.7	0.669
NUS	5	1.051	0.239	0.182	0.150	(Mg)3.43	1.0526
NUS (RG)	5	1.144	0.083	0.223	—	(Mg)3.43	1.0526
IMRE	2	0.746	0.136	0.063	—	(Al)2.15	0.592
IMRE	2	0.870	−0.090	0.084	—	(Al)2.7	0.78
CSIR	2	0.943	−0.134	0.099	0.037	(Al)3.448	1.000
CSIR (RG)	2	0.981	−0.238	0.120	—	(Al)3.448	1.000
EMPA	2	1.016	−0.017	0.069	0.026	(Al)3.491	0.915
EMPA (RG)	2	1.056	−0.085	0.080	0.065	(Al)3.491	0.8469(100) 0.8541(111)
NPL (RG)	5	0.998	0.025	0.019	0.029	(Mg)2.964	0.9329
Philips AR 0–45°	5	1.223	0.977	0.084	0.020	(Al)3.90	0.75
Philips AR 0–60°	5	1.108	0.333	0.054	0.020	(Al)3.90	0.75
Philips QT, 10°	1	1.470	0.634	0.213	0.230	(Al)	
Philips QT, 35°[b]	1	1.542	0.751	0.256	0.369	(Al)	
Philips AOS, 10°[b]	1	1.316	1.526	0.149	0.167	(Al)	
Philips AOS, 35°[b]	1	1.419	1.968	0.227	0.237	(Al)	
Philips RG1	2	1.003	0.167	0.075	—	(Al)3.448	0.933
Philips RG2	2	0.987	0.426	0.081	—	(Al)3.448	0.933
Average[c]		1.045	0.172	0.105			
SD[c]		0.145	0.369				

[a] RG = reference geometry; AR = angular resolved; QT = QUASES-Tougaard algorithm; AOS = AOS algorithm.

[b] Lower thicknesses only.

[c] Excluding Philips QT and AOS.

The thickness is then obtained from the regression plot of $\ln(1 + R_{expt}/R_o)$ versus $\sec\theta$ for $\theta \leq 50°$, with an added point at the origin. The uncertainties in this fit were in the range 2–8%. The NRC later conducted the work also using the reference geometry.

The m, c and r values from the fits to the NPL thickness data are given in Tables 7 and 8. The major change between the original data and the revised data sets arises from the use, in the first set, of the gradient of $\ln(1 + R_{expt}/R_o)$ versus $\sec\theta$ to determine d. This method usually leads to a bias, as described earlier. This bias may increase or decrease m and change the offset c. If we use the alternative approach of averaging the deduced values of d for $0° \leq \theta \leq 60°$ using the NRC values of R_o and L_{SiO_2}, the values of m and c are 1.017 and −0.283 nm, respectively. The value of m is closer to unity but the offset has increased. The negative offsets here are to be expected from the non-standard methods of background subtraction.

The third set of XPS data is from the Materials Characterization Division, National Metrology Institute of Japan (NMIJ), using a VG Escalab 220i instrument with monochromated Al Kα x-rays incident at 54° from the surface normal and with the emitted electrons detected along that normal. The Si 2p peak areas for the elemental and SiO_2 states were measured between fixed energies after removal of a Shirley background. Values of R_o and L_{SiO_2} were deduced from GIXRR measurements for six NMIJ materials. The GIXRR study gives a thickness d_G. We shall discuss GIXRR in a later section. From Eqn. (1) we then have

$$R_{expt} = R_o \exp\left(\frac{d_G}{L_{SiO_2}\cos\theta} - 1\right) \qquad (12)$$

and a plot of R_{expt} versus d_G gives $R_o = 0.70$ and $L_{SiO_2} = 3.39$ nm, respectively. Using these values, the m, c and r values from the fits to the NPL thickness data are shown in Tables 7 and 8. As before, for this geometry where

Table 8. The XPS results using consistent values of L_{SiO_2} (Mg) = 2.964 nm, L_{SiO_2} (Al) = 3.448 nm and $R_o = 0.933$

Laboratory	m	c (nm)	r (nm)	A at 0°	Emission angle
BAM	1.065	−0.241	0.113	1.83 nm	0°
BAM (RG)[a]	0.995	0.026	0.052	—	RG
NRC	1.004	−0.304	0.119	—	0–50°
NRC (RG)	0.981	−0.171	0.094	—	RG
NMIJ	0.976	−0.465	0.100	>3.45 nm	0°
University of Utsunomiya	0.993	−0.156	0.146	—	10–55°
University of Utsunomiya (RG)	1.030	0.043	0.084	—	RG
NTT	1.062	−0.160	0.107	—	45°
NIMS	0.954	−0.234	0.092	1.48	0°
PSB	1.014	−0.084	0.086	—	0°
NUS	1.082	−0.349	0.093	—	0–60°
NUS (RG)	1.036	0.012	0.136	—	RG
IMRE	1.054	−0.292	0.119	2.47	0°
CSIR	0.962	−0.082	0.096	—	0–70°
CSIR (RG)	1.000	−0.178	0.115	—	RG
EMPA	1.000	−0.035	0.069	—	45°
EMPA (RG)	1.018	−0.177	0.084	—	RG
NPL (RG)	0.998	0.025	0.019	—	RG
Philips (0–45°)	0.996	0.032	0.053	—	3–45°
Philips (0–60°)	0.976	0.135	0.045	—	3–60°
Philips (RG1)	0.952	0.101	0.056	—	RG
Philips (RG2)	0.969	0.128	0.054	—	RG
Average (not RG)	1.011	−0.127	0.095		
SD (not RG)	0.040	0.194			
Average RG	1.001	−0.013	0.071		
SD RG	0.026	0.110			

[a] RG = reference geometry.

the angle of emission is along the surface normal, we see a significant and negative offset value for c. We shall see later that this use of GIXRR, if corrected in a certain way, would lead to $R_o = 0.78$ and $L_{SiO_2} = 3.39$, which are close to the values expected for emission along the surface normal.

The fourth set of XPS data are from the University of Utsunomiya using a PHI ESCA 5600 instrument with a focused monochromatic Al x-ray beam incident at 45° to the surface normal. The emitted electrons are detected at 10°, 32°, 45°, 55°, 65°, 73° and 80° from the surface normal. The spectra had the background removed and the remaining Si 2p peaks were fitted by one peak each for the elemental and oxide states for determining the intensities. The elemental peak is usually fitted with two peaks to ensure a good fit to the asymmetry of the spin-orbit splitting, but this was not done here. Using one peak is not generally recommended, although it is highly likely that the positive and negative errors largely cancel. Whether they do or not depends on the software designers choosing either to minimize the square of the residuals or of chi (the residuals divided by the standard deviations). In this work, the thickness is calculated as the average for each emission angle, and because a fall-off in calculated thickness is observed for $\theta > 60°$, as expected from elastic scattering theory,[3,72] the data are restricted to $\theta < 60°$. The value of L_{SiO_2} is taken directly from the IMFP of Tanuma *et al*.[33] to be 3.77 nm. Two values of R_o were used. Direct calculation gives $R_o = 0.525$, which is a value close to that reported earlier.[20] However, direct measurements of a thick thermal oxide and an etched wafer here gave $R_o = 0.8756 \pm 0.0004$ as the average for measurements at 10°, 45° and 65° angles of emission. Measurements subsequently were made for the reference geometry. The m, c and r values from the fits to the NPL thickness data are given in Tables 7 and 8. The use of the calculated value of R_o leads to unrealistically high values of both m and c. Using the consistent values of R_o and L_{SiO_2} in Table 8, however, does lead to low offset values and good repeatabilities, with those at the reference geometry being particularly good.

The fifth set of XPS data are from the Centre for Materials Analysis Technology, NTT Advanced Technology Corporation, using a PHI 5700 instrument with a focused monochromatic Al x-ray beam incident at 45° and with the detected electrons also at 45° to the surface normal. The spectra had the background removed by fitting a Shirley background[32] separately to Si 2p peaks of the elemental substrate and the SiO_2 overlayer in order to determine the peak areas. No peak fitting was conducted to determine the area. This approach was not used elsewhere where single Shirley backgrounds were always applied. There are two differences that cause several very small changes.[6] Because

the background matching point is placed between the peaks, the intensities of the interface oxides are removed. However, it is also clear that the Shirley backgrounds for the two peaks should not be the same[6] because the elemental state (as in this case) is relatively stronger. Fortunately, these changes cause relatively small effects in the deduced thicknesses.[6] The thicknesses were calculated again using Eqn. (1) with L_{SiO_2} put equal to the IMFP value of 3.77 nm from Tanuma *et al*.[33] The intensities for pure SiO_2 and Si were measured with each sample using two extra samples, a thick oxide cleaned with $H_2O_2 + H_2SO_4$ solution and bare silicon cleaned by sputtering. These values gave $R_o = 0.8278 \pm 0.0482$. The m, c and r values from the fits to the NPL thickness data are given in Tables 7 and 8. The reduction of L_{SiO_2} from the IMFP value of 3.77 nm to the common attenuation length value of 3.448 nm reduces the value of m by 10% and the increase of R_o to 0.9329 reduces both m and the offset further.

The sixth set of XPS data are from the Materials Physics Group, National Institute for Materials Science (NIMS), using a home-built spectrometer with Mg x-rays incident at 48.5° and detected electrons along the surface normal. The spectra had x-ray satellites and a single Shirley background removed in order to determine R_{expt}. The thicknesses again were calculated using Eqn. (1), based on a calculated value of R_o. This value is similar to that calculated earlier but has extra factors f_{SiO_2} and f_{Si} to allow for surface excitations. Thus

$$R_o(\text{NIMS}) = R_o(\text{calc})\frac{f_{SiO_2}}{f_{Si}} \tag{13}$$

where, for f_{SiO_2} and f_{Si}

$$f = \exp(-aE^{-b}) \tag{14}$$

with $a_{Si} = 1.7$,[69] $b_{Si} = 0.29$,[69] $a_{SiO_2} = 0.5124$[70] and $b_{SiO_2} = 0.4071$.[70] For a peak energy of $E = 1154$ eV, the ratio f_{SiO_2}/f_{Si} is 1.210 so that $R_o(\text{NIMS}) = 0.678$. This value is closer to the experimental values than that previously calculated and effects of this type, usually neglected, may account for part of the difference found earlier. In the above, Ref. 69 evaluates a and b for Ni and the values for Si are assumed to be the same here. However, if the earlier values of Kwei *et al*.[70] for Ni are used ($a = 1.9411$ and $b = 0.4533$), f_{SiO_2}/f_{Si} is 1.052 and R_o falls to 0.59. The value of L_{SiO_2} is taken as 3.07 nm, being the average for 2–8 nm layers calculated from the NIST database.[74] The fits to the NPL data are given in Tables 7 and 8. Note in Table 8 that the use of the 0° emission, along a forward focusing direction, has led to a negative offset very similar to that observed for the data from BAM.

The seventh set of XPS data are from the PSB Corporation using a VG Escalab 220i XL instrument with monochromatic x-rays incident at 58° and detected electrons along the surface normal. The analysis was conducted using two peaks via Eqn. (1), with L_{SiO_2} taken as an attenuation length of ~2.7 nm and R_o from the data of Shallenberger *et al*.[75] as 0.669. The m, c and r values from the fits to the NPL thickness data are given in Tables 7 and 8. Note that here, using the reference values for L_{SiO_2} and R_o in Table 8 leads to a marked improvement in both m and c. The small size of the negative offset for normal emission for c here may arise from the large solid angle for the VG Scientific 220i XL instrument with its magnetic input lens. This still emphasizes the need to work away from 0° emission because the effects, as described earlier, are expected to be dependent on the solid angle of analysis and this may depend on the instrument operational settings.

The eighth set of XPS data are from the NUS using a VG Escalab II instrument with Mg x-rays incident at 49° when the electron emission is along the surface normal. Spectra were recorded for 0°, 15°, 30°, 45°, 55° and 60° angles of emission. The spectra were not subject to Mg x-ray satellite removal. A straight-line background was removed and the spectra were fitted to four peaks, each with a spin-orbit component at 50% intensity and 0.6 eV higher binding energy. The peaks were Si, Si_2O (1.00–1.01 eV higher BE), Si_2O_3 (2.49–2.51 eV higher BE) and SiO_2 (4.23–4.30 eV higher BE). Peak synthesis analysis showed no significant SiO (expected at 1.8 eV higher BE). The thicknesses were determined from plots of $\ln(1 + R_{expt}/R_o)$ versus $\sec\theta$, from which the gradient should be d/L_{SiO_2}. The value of R_o was determined experimentally to be 1.0526 from data recorded at normal emission. Here, data for $I^{\infty}_{SiO_2}$ were measured for a thick thermal oxide and I^{∞}_{Si} for a sputter-cleaned Si(100) sample. The value of L_{SiO_2} was calculated using the NIST attenuation length database[74] with a density of 2.27 g cm^{-3} and a bandgap of 9 eV. This gave an L_{SiO_2} value of 3.43 nm. In the plots, the intensities for all oxide peaks were summed to generate a total oxide intensity for R_{expt}. This is not the same as the five-peak method described for Eqns (2)–(6). The plots showed a non-zero intercept, with the intercept on the $\ln(1 + R_{expt}/R_o)$ axis being positive for the thinner samples and negative for the thicker samples. This arises from the effects of forward focusing in the Si wafer substrate. The m, c and r values from the fit of the reported thicknesses to the NPL thickness data are given in Table 7. The offset to the plots of $\ln(1 + R_{expt}/R_o)$ versus $\sec\theta$, seen here, leads to thickness values that are too low at low d values but about right for the thicker samples, so that m would be above unity and c negative in Table 7 if the reference values for L_{SiO_2} and R_o had been used. In Table 8, the data are recalculated according to Eqns (2)–(6) using the reference values for R_o and L_{SiO_2}, with the thicknesses then being averaged over the six emission angles. After the first study, the measurements were repeated at the reference geometry, as shown in Tables 7 and 8. In Table 8 we now see an m value close to unity and an offset significantly smaller than the measurement repeatability.

The ninth set of XPS data is from the Materials Science and Characterization Laboratory, Institute of Materials Research & Engineering (IMRE), using a VG Escalab 220i instrument with the emitted electrons detected along the surface normal. The data are analysed using Eqn. (1) with two possible values for L_{SiO_2} and R_o. In the first case, $L_{SiO_2}\cos\theta$ is taken as 2.15 nm and R_o as 0.592. In the second case, $L_{SiO_2}\cos\theta$ is 2.7 nm and R_o is measured experimentally to be 0.78. The measurements for R_o were made using a lightly sputtered 100 nm thermal oxide and an unsputtered hydrogen-terminated etched Si(100) wafer. The m, c and r values from the fits of the reported thicknesses to the NPL thickness data are given in Table 7, with recalculations in Table 8. Here, again, use of the 0°

emission angle leads to a negative offset in Table 8 and the low value of R_o determined experimentally.

The tenth set of XPS data is from the National Metrology Laboratory of South Africa (CSIR), using a PHI Quantum 2000 instrument with monochromatic x-rays incident at an angle equal to 45° minus the electron emission angle. Spectra were recorded for 0°, 30°, 45°, 60°, 70°, 75° and 80° emission angles and the peak areas were determined for SiO_2 and Si after removal of a Shirley background. The SiO_2 peak was fitted with one peak and the Si by an unconstrained pair of peaks. The Shirley background fit used in this analysis was a non-iterated Shirley background that 'looked' good but in some cases exhibited a non-satisfactory result, as discussed in work to test the fitting of algorithms.[9] The oxide thicknesses were calculated using Eqn. (1) with $L_{SiO_2} = 3.448$ nm[20] and $R_o = 1.000$. The thicknesses measured at different emission angles were averaged, excluding the 75° and 80° data and any other angles for which either the SiO_2 or Si intensities were too small. The m, c and r values from the fits to the NPL thickness data are given in Tables 7 and 8. After the initial study, the data were repeated at the reference geometry. Further data were analysed using an iterated Shirley background. This led to small changes in the thicknesses, typically ~2%, the latter being the measurement precision of the data in this set. This in turn led to small changes in the m and c values. The data in Tables 7 and 8 for the initial 'as-received' data use the non-iterated background, whereas those for the reference geometry are for the iterated background.

The eleventh set of XPS data is from the Applied Technology and Development Group at the Swiss Federal Laboratories for Materials Testing and Research (EMPA), again using a PHI Quantum 2000 instrument with monochromatic x-rays and an electron emission angle of 45°. The SiO_2 and Si peak areas were obtained by peak fitting with two peaks after subtraction of a Shirley background. The thicknesses were calculated from Eqn. (1) using an IMFP of 3.77 nm[33] and an L/IMFP ratio of 0.926[72] for SiO_2 at 1305 eV to give $L_{SiO_2} = 3.491$ nm. The value of R_o was measured experimentally to be 0.915 by using a thermal oxide 33 nm thick and measuring $I^{\infty}_{SiO_2}$ and I^{∞}_{Si} after 4 and 44 nm of sputtering, respectively. The m, c and r values from the fits to the NPL thickness data are given in Tables 7 and 8. After the initial study, the data were repeated at the reference geometry. Here, individual R_o values were determined at the reference geometry: $R_o = 0.847$ for the (100) wafers and $R_o = 0.854$ for the (111) wafers.

The twelfth set of XPS data is from the NPL using the method described at the start of the Results section and Eqns (2)–(6). This extra set of data were recorded for a new sample using the reference geometry and appears only in Table 8.

The thirteenth set of XPS data is from Philips using a PHI Quantum 2000 instrument with monochromated Al x-rays. Here, several different methods were used. The first method used data recorded at angles of emission of 0°, 3°, 10°, 20°, 30°, 40°, 45°, 50°, 55°, 60°, 65°, 70° and 75°. The Si 2p peaks were analysed by peak synthesis after removal of a single Shirley background for the five peaks, as described earlier, allowing for spin-orbit splitting of 0.6 eV with the $2p_{1/2}$ peak at 50% of the $2p_{3/2}$ intensity. The oxide thickness then was calculated using Eqn. (1), where the oxide intensity was taken as the sum of the SiO_2 and intermediate oxide intensities. The value of R_o was taken as 0.75[12] and L_{SiO_2} was taken to be the IMFP from the TPP-2M formula[5] at 3.90 nm. Plots using this approach of d versus θ showed effects similar to those described earlier[20,26] in which d increases slowly with θ to a peak at ~40° and falls significantly beyond 60° as a result of elastic scattering effects. Data therefore were analysed with a more complex theoretical analysis including elastic scattering[19] but ignoring the data at 0° that involved diffraction effects. The value of 0.75 for R_o was taken from experimental measurements in the literature[12] and was preferred to the lower value calculated theoretically. Using this approach generates values of d that give the m and c values of Table 7. These data have been re-evaluated for the method involving Eqns (2)–(6) and averaging the d values for $\theta \leqslant 45°$ and $\theta \leqslant 60°$ using the common L_{SiO_2} and R_o values, as listed in Table 8.

This study at Philips also used the two methods based on electron transport described in the section on XPS to determine the O 1s photoelectron peak intensity with its background. The result is given in Table 7 for 10° and 35° emission angles using the QUASES-Tougaard (QT) algorithm and the much simpler 'AOS in 3λ' algorithm, respectively. For the QUASES-Tougaard method at 10° the result is very well behaved. The value of $m = 1.47$ is rather high but the thicknesses are quite linear with the NPL reference values over the full range of thicknesses. We expect, in this method, an offset c similar to that for RBS or MEIS because here we are also measuring an oxygen thickness that includes the contamination overlayer. The offset ($c = 0.634$ nm) is indeed similar and when the thicknesses are calibrated against the NPL reference values the offset becomes $0.634/1.47 = 0.429$ nm. The depth probed accurately with QUASES-Tougaard is $\sim 5\lambda_{O1s}\cos\theta$. At 35° emission angle the largest depths have been omitted in the analysis in Table 7 and the results are quite similar to the results at 10°. Because only one of the participating laboratories used the QUASES-Tougaard method, a standard uncertainty of the method cannot be determined. Table 7 also shows the result of the 'AOS in 3λ' analysis. This is a simplified and less accurate version of the more elaborate QUASES-Tougaard algorithm. Here the depth probed is limited to $\sim 3\lambda_{O1s}\cos\theta$ and the determined thickness will gradually saturate for film thicknesses in the range above $2\lambda_{O1s}\cos\theta$.[71] When the data above $2.5\lambda_{O1s}\cos\theta$. (i.e. above 5 nm) are eliminated, the results are similar to the QUASES-Tougaard method. The larger offset is a natural consequence of the above-mentioned saturation effect when data are fitted to a straight line.

After completing this work, the analysis was repeated using the reference geometry for two PHI Quantum 2000 instruments, as shown in Tables 7 and 8. Here, as before, in Table 7 the intensities for SiO_2 and the interface oxides were summed to use in Eqn. (1), whereas in Table 8 Eqns (2)–(6) are used.

To check on the measurements for the total oxygen by other methods, we may use the O 1s peak. Intensities for the

O 1s peak were obtained in the original widescans for the ten NPL basis samples and were quantified according to Eqn. (10) applied to the O 1s peak instead of the Si 2p oxide state peak. For this we also need the O 1s absolute intensity for a thick oxide layer, I^{∞}_{O1s}, and to ensure consistent absolute intensities from sample to sample. This has greater uncertainties than the approach using the ratio of the 2p peak areas within each spectrum. Nevertheless, the data correlate well using the value of 2.028 nm for L_{SiO_2} for the O 1s electrons at a kinetic energy of 722 eV using Mg x-rays.[20] The correlation has a gradient of unity and an offset, evaluated for samples <5 nm thick, of 0.35 ± 0.15 nm. The oxygen peak thus indicates an oxygen-containing contamination layer with this equivalent thickness that is not a compound of silicon. This is thought to be chemisorbed water. The results for samples thicker than 5 nm are less certain because they depend very sensitively on I^{∞}_{O1s} remaining constant between samples to within 1%.

Ellipsometry

Ellipsometry is one of the most popular methods for thin-film measurement, and certified reference materials (CRMs) of SiO_2 on Si are sold for calibrating the method.[76,77] However, these materials are generally used at thicknesses greater than 50 nm. The thinnest reference material is 10 nm[76] and here the user is warned that contamination layers accumulate and need to be removed by a defined cleaning procedure. Ellipsometry has favour because it is fast, economic and very precise. As discussed in the section on preparation of the samples, maps of all the wafers used in this and other work were recorded very quickly with precisions around 0.002 nm. In the studies presented here, the ellipsometry is either conducted at one wavelength such as the HeNe laser wavelength of 632.8 nm or as spectroscopic ellipsometry over the wavelength range $200 < \lambda < 850$ nm and angles of incidence near 70°.

In its most basic terms an ellipsometer measures, under specular reflection conditions, the change in the phase difference between the parallel and perpendicular components of the light beam upon reflection, Δ, and the ratios of the outgoing wave amplitudes to the incoming wave amplitudes for these components, respectively. The ratio of the latter gives tan Ψ and it is Δ and Ψ that are generally measured. For transparent films in Δ, Ψ space, the coordinates form a trajectory starting from $\Delta \sim 178.5°$ and $\Psi = 10.5°$, moving approximately in an elliptical manner anticlockwise.[78,79] For films up to 10 nm thick, the trajectory is towards $\Delta = 150°$ with less than a degree change in Ψ. The precise trajectory in Δ, Ψ space may be calculated using the known optical constants for the SiO_2 overlayer and the Si substrate. Thus, for a perfect layer of SiO_2 on Si all of the optical parameters are known and the thickness may be determined. Issues that are not easy to address are the effects of the interface oxides, which are small, and of the contamination overlayers, which are generally unquantified.

The first set of data was from the Physikalisch-Technische Bundesanstalt (PTB), using a SOPRA (ESVG) spectroscopic ellipsometer with the light incident at 75° to the normal and for $300 < \lambda < 850$ nm to measure the ellipsometric parameters. The thicknesses were calculated with the instrument software using optical data for SiO_2[80] and for the two substrates Si(100)[81] and Si(111).[81] From 1997 until now, a standard deviation of 0.2 nm has resulted from single measurements at the PTB. In this work TEM studies were also made, as reported later. It was recognized that the ellipsometry would include hydrocarbon and water layers and so a fixed amount would need to be subtracted from all the thicknesses. The TEM measurements for the 2 nm and 4.5 nm oxides on (100) substrates gave thicknesses smaller than for ellipsometry by 0.386 nm and 0.407 nm, respectively. The ellipsometric data, therefore, were reduced by 0.395 nm and, when compared with the NPL thickness data, gave m, c and r values as in Table 9 but the c value for the PTB-corrected ellipsometric measurement reported was 0.584 nm (i.e. 0.979 nm minus 0.395 nm). The uncorrected offset is shown in Table 9 with a footnote to indicate the value reported. We present the data in this mode to indicate the results for each technique separately. We expect there to be a minimum carbonaceous contamination of ~0.25 nm if the material is kept clean, and also water adsorption in excess of one monolayer because the ellipsometry, unlike other methods, is conducted in air. An offset of at least 0.6 nm is therefore expected.

The second set of data was from BAM, using an RAE spectroscopic ellipsometer with the light incident at 65°, 70° and 75° to the normal for $270 < \lambda < 1100$ nm to measure the ellipsometric parameters. The thicknesses were calculated using a single layer on a substrate model, with thermal oxide data for SiO_2 and Si taken from Jellison.[81] The fitting was made to d and then to the optical constants. No relevant changes to d were observed from the changes caused by the fitting to the optical constants. Experience with measurements of this type indicate a statistical contribution to the uncertainty of the order of 0.01 nm, but the type B

Table 9. Ellipsometry and spectroscopic ellipsometry results

Laboratory	m	c (nm)	r (nm)	Repeatability (nm)
PTB	0.985	0.979[a]	0.051	0.015
BAM	0.975	1.031	0.049	—
NTT	0.980	0.869	0.091	—
KRISS	1.003	0.726	0.050	0.018
NUS	0.963	1.276	0.111	0.013
NPL	0.993	0.480	0.089	—
University of Leipzig	0.994	1.054	0.136	—
NIST-1	0.991	1.180	0.046	0.007
NIST-1 thermal preclean	0.990	0.936[b]	0.082	—
NIST-2 thermal preclean	0.990	0.806[b]	0.130	0.109
Average	0.986	1.016[c]	0.084	
SD	0.011	0.174[c]		

[a] The PTB-corrected ellipsometry results reported have an offset c of 0.583 nm, as described in the text, to allow for the 0.396 nm surface contamination as measured at PTB by TEM.

[b] Samples thermally precleaned before measurement.

[c] Value excluding the NPL data, which were for the samples prior to distribution, and data for the thermally precleaned samples (c for thermally precleaned samples $= 0.871 \pm 0.092$ nm).

contribution is of the order of 0.2 nm at a 95% confidence level. The *m*, *c* and *r* values from the fits to the NPL thickness data are given in Table 9.

The third set of ellipsometry data is from NTT Advanced Technology Corporation and originally was made simply to check the XPS data, presented earlier, using a SOPRA MOSS ES4C spectroscopic ellipsometer with an angle of incidence of 74.95° and $300 < \lambda < 850$ nm. The fit to the NPL data are given in Table 9 and again we see an *m* value close to unity but an offset close to 1 nm. The fourth set of ellipsometry data are from KRISS, using an ISA UVISEL phase-modulated spectroscopic ellipsometer at 70° angle of incidence and $250 < \lambda < 830$ nm. Here the usual three-phase model of air, SiO_2 and Si substrate is used, with the refractive index of Si from Yasuda and Aspnes[82] and that for amorphous SiO_2 from the dispersion equation for fused silica.[80] Two runs were made and the average taken. The *m*, *c* and *r* values from the fits to the NPL thickness data are given in Table 9. The scatter between the two runs was comparable to the value of *r* in Table 9. Again we see *m* very close to unity and *c* with a smaller offset of 0.726 nm. The fifth set of ellipsometry data were recorded by the NUS using a Woolam VASE instrument with three incidence angles, 65°, 70° and 75° for $300 < \lambda < 1200$ nm. The model and input data here are the same as used at KRISS. The *m*, *c* and *r* values from the fit to the NPL thickness data are given in Table 9. The *r* value there is generally lower than the average 0.190 nm estimated from the goodness of fit of the data for Δ and Ψ. The repeatability is much better at 0.013 nm. The sixth set of ellipsometry data were recorded for the NPL as part of the original diagnosis using an ellipsometer designed for wafer production line mapping. This was for a Philips PZ 2000 instrument using the HeNe line at 632.8 nm, incident at 70°. The calculations use self-contained data sets in the instrument software. The *m*, *c* and *r* values from the fits to the NPL thickness data are given in Table 9. The offset is low here because the samples had been made only recently and had been kept in the dust-free environment.

The seventh set of ellipsometry data was from the University of Leipzig using a Woolam VASE instrument with two incidence angles of 68° and 70° for $310 < \lambda < 1240$ nm. An example of the data and fits to theoretical curves for the optical parameters are shown in Fig. 12. The quality of the fits leads to a total uncertainty of 0.05 nm and indicates that the film is of the correct stoichiometric SiO_2 and that any interface oxide layer is no more than the thickness of 0.15 nm predicted theoretically.[83] For these calculations the simple model is described by Azzam and Bashra[84] and the values of the Si and SiO_2 optical constants for the fits to the optical data are taken from Herzinger *et al.*[85] The *m*, *c* and *r* values from the fits to the NPL thickness data are given in Table 9.

The eighth and ninth sets of ellipsometry data were from the National Institute of Standards and Technology (NIST-1). In this study, a fully characterized home-built instrument was used, based on a rotating analyser with an Xe source at 75° to cover the range 1.5–6.0 eV in steps of 0.05 eV (i.e. $210 < \lambda < 830$ nm). The first set of data were recorded for untreated samples and the second, to desorb contaminants, was from samples heated to 500 °F

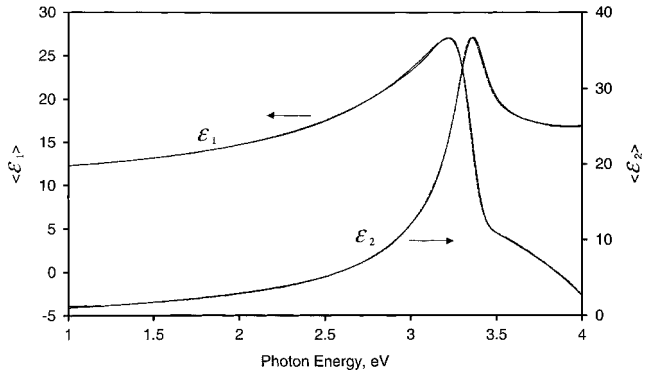

Figure 12. Ellipsometric spectra from the University of Leipzig for the pseudodielectric function $\langle\varepsilon_1\rangle + i\langle\varepsilon_2\rangle$ measured and calculated for two angles of incidence for the 4.5 nm oxide on Si(100). The energy range 1–4 eV corresponds to wavelengths of 1240–310 nm.

(260 °C) for 3 min with the data recorded immediately after a quench onto copper at room temperature. A similar approach for XPS[21] indicates that this may reduce the carbonaceous contamination thickness by 0.1 nm. The same three-phase model as used above was used here, with the optical constants for Si from Johs[86] and for SiO_2 using the Bruggemann effective medium approximation to obtain an equivalent index of 1.461 at 632.8 nm wavelength. The *m*, *c* and *r* values from the fits to the NPL thickness data are given in Table 9. Note that the offset *c* is similar to the other values and that heating reduces this by 0.24 nm. This is significant but still leaves a considerable offset remaining. The 90% confidence limit from the fitting of the data averages 0.12 nm and the standard deviation of the repeatability is only 0.007 nm. If the uncertainty of the refractive index is 0.002, which is measurable by ellipsometry, the uncertainty in the film thickness is 0.3%. The use of various published dielectric functions leads to thickness variations of 2.4% in the worst case. The uncertainties in the geometries lead to uncertainties significantly less than this value. The total uncertainty at 90% confidence is thus 0.13 nm for the thinnest oxide, rising to 0.23 nm for the 8 nm oxide.

At NIST, the tenth set of ellipsometric data was recorded separately (NIST-2) using a high-accuracy single-wavelength ellipsometer with the HeNe line at 632.8 nm incident at 75° to the surface normal. The samples here were also heated for 3 min, face up on a clean hot plate at 500 °F followed by a quench onto copper for 1 min and then measured within a few minutes. This showed that a layer equivalent to 0.2 nm of oxide was removed. The refractive index used for the Si substrate is 3.8738 + i0.01452 and for the oxide it is 1.4617, calculated using the effective medium approximation with 101% SiO_2 and −1% voids to allow for typical compressive stress in this oxide. This thickness will include the interface oxides and contamination. The system was designed for wafers of 2″ or greater diameter. A special holder was made for these smaller samples, limiting the repeatability to 0.1 nm instead of the more usual 0.004 nm. This was the main uncertainty. The *m*, *c* and *r* values from the fits to the NPL thickness data are given in Table 9.

Before leaving the ellipsometry section, it is worth noting in summary that the precision here is very good and that the ten values of m give $m = 0.986 \pm 0.011$, where the uncertainty is the standard deviation of the scatter. The fits of the data for spectroscopic ellipsometry confirm that the material is consistent with the bulk thermal oxide and this supports the XPS data, which showed that the oxygen content of the thermal oxide differed from that of single-crystal SiO_2 by $1.6 \pm 2.1\%$ at one standard deviation.[20] If we take the ten values as being estimates of a true value of m, then the value of m is 0.986 with a standard error of the mean of ± 0.004 at one standard uncertainty.

Grazing-incidence x-ray reflectometry and neutron reflectometry

Whereas the analytical techniques mainly provide the amount of substance as atoms m^{-2}, GIXRR and neutron reflectometry are length-measuring methods and, by the same process as traditional interferometry, the thickness d may be deduced via the simple relation

$$n\lambda = 2d\cos\theta \tag{15}$$

where λ is the wavelength of the radiation at an angle of incidence θ from the surface normal. Of course, λ and θ here are the values in SiO_2, not in the vacuum, although the refractive index is very close to unity. Minima or maxima in the reflected intensity are separated by increases in the n value of unity.

In the first study at the PTB, GIXRR was conducted at the BESSY II storage ring in Berlin in ultrahigh vacuum. At the beam energies normally used for film thickness measurement, ~8 keV, the contrast between SiO_2 and Si is poor and so the accuracy is not good. Contrast was enhanced significantly by working at a photon beam energy just above the Si K absorption edge at 1841 eV,[87] with a wavelength λ of 0.674 nm. Measurements of reflectance then were made as the angle of incidence was decreased from 90° to 81°. For the thicker oxides this leads to a series of minima from which the thickness may be deduced. Rather better accuracy is achieved by a full modelling of the reflectance. In this way, the precision for the thicker films where there are several sharp minima (as shown in Fig. 13) is excellent, but the precision for the thinner films is poorer. Overall, the uncertainty estimated from fitting the full reflectometry curves is 0.2 nm for the 5 and 8 nm samples, rising to 0.3 nm for the 4 nm sample analysed. A small part of this uncertainty arises from the contamination, which has similar optical properties to the SiO_2 at this wavelength, and partly from uncertainties in the refractive index of the SiO_2 at this wavelength. Work is continuing at BESSY II to determine more accurate refractive index data. Fewer samples were analysed because the beam time at BESSY II is restricted. The m, c and r values from the fit to the NPL thickness data are given in Table 10. In this fit, the precision of the thicker oxides was better than that for the thinner oxides and so a weighted fit has been used, with the weighting varying inversely with the measurement variance. Comparisons for thicker samples of a different batch have been made independently within the PTB. For samples in the range 6–1000 nm, the ratio of the m values from GIXRR and ellipsometry in these two laboratories was 1.009,[87] which is very close to the value of 1.015 found here for the shorter range of 4–8 nm.

In the second GIXRR study at the NMIJ, a high-resolution Rigaku ATX-G2 rotating anode diffractometer was used in air. The Cu Kα x-rays at a wavelength λ of 0.154 nm were monochromated using a channel-cut Ge(220) monochromator.[88] The interference concept is the same as that given above but the higher energy x-rays lead to poorer contrast and hence a need to model the intensities very carefully using the method of Parratt,[89] with roughness included as described by Sinha *et al.*[90] The layers were modelled as pure SiO_2 on an Si substrate but with carbonaceous contamination. The measurements for the repeatability analysis showed a detectable increase in apparent film thickness of 0.2 nm after 2 days of work. It was assumed that all samples accumulated carbon during the study and, because the density of this overlayer is approximately half that of SiO_2, the increase in the GIXRR thickness is assumed to be approximately half of the carbonaceous contamination thickness. The carbonaceous contamination thickness was measured by XPS after the GIXRR data were recorded and quantified using parameters for an organic polymer. This led to the removal of 0.16 nm, with an estimated uncertainty of 0.1 nm, from each GIXRR

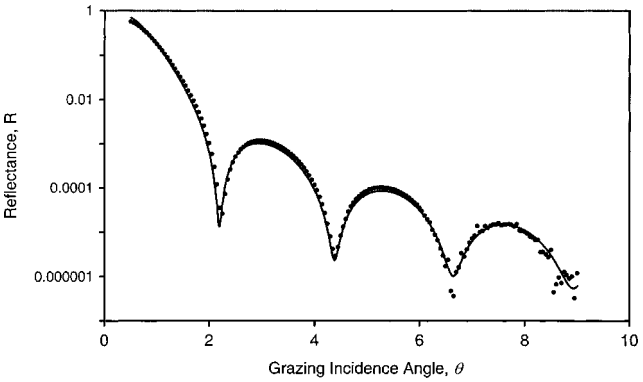

Figure 13. The GIXRR response as a function of the angle (in degrees) from the surface for the 8 nm oxide on Si(100) measured at BESSY II by the PTB using 1841 eV photons. The smooth curve is the fit with the roughnesses of the SiO_2 surface and the SiO_2/Si interface at 0.24 and 0.42 nm, respectively.

Table 10. The GIXRR and neutron reflectometry (NR) results

Laboratory	m	c (nm)	r (nm)	Repeatability (nm)
NIST (NR)	0.991	0.185	0.026	
PTB (GIXRR)	0.970	0.548	0.070	
NMIJ (GIXRR)	0.974	0.554[a]	0.188	0.073
GIXRR average	0.972	0.551	0.084	
GIXRR SD	0.003	0.004		

[a] GIXRR results reported give 0.394 nm, as described in the text, to allow for 0.16 nm contributed by the carbonaceous contamination as measured by XPS.

result. The m, c and r values from the fit of these data to the NPL thickness data are given in Table 10. We see a rather less precise result than at the PTB, where the lower energy gave improved contrast but a lower offset arising from removal of the carbonaceous contamination.

In the third of these interference studies, at NIST, neutron reflectometry is conducted as described by Dura *et al.*[91] using a neutron beam at a wavelength λ of 0.475 nm. The behaviour is similar to GIXRR. The specular intensity has maxima and minima as a function of the angle of incidence θ from 78° to 90°, arising from the interference of neutrons scattered from the upper and lower interfaces of the oxide. In general, neutron reflectometry gives superior contrast to GIXRR because the scattering depends on the nuclear structure, whereas in GIXRR it is, to first order, proportional to atomic number Z. Neutron reflectometry is thus less sensitive to the carbonaceous and water contaminations. To improve the contrast in GIXRR the beam energy needs careful selection, as discussed above. In the neutron reflectometry work, the formalism of Parratt[89] was used with the program of Ankner and Majkrzak[92] and with parameters for the materials given in the literature.[93] In the fitting, a number of parameters are allowed freedom, including the roughnesses of the surface and the interface. However, these fits all give a very tight range for the oxide thickness because the frequency of the minima is almost completely independent of these other parameters. The uncertainty is thus almost completely defined by the statistical quality of the fits. Figure 14 shows fits for the 8 nm oxide on Si(100) of thickness 8.04 ± 0.01 nm with various different models for the contamination overlayer. A simple estimation from the minima gives a value within 0.4% of this value. In this work only the 2 and 8 nm (100) and 2 and 6 nm (111) samples were analysed. The uncertainties were, respectively, 0.15, 0.01, 0.05 and 0.03 nm. These values encompass the full range of all the possible fits for each sample and so may be considered as 95% confidence levels. The m, c and r values from the fit to the NPL thickness data, using the weighting for the above uncertainties, are given in Table 10. The associated standard uncertainties are 0.008 for m and 0.050 nm for c. The 2 nm (100) material has the poorest uncertainty and, if it is not included in the fit in Table 10, m increases to 0.999, c falls to 0.138 nm and r to 0.023 nm. If the data are unweighted, the m and c values change to 0.988 and 0.211 with an rms scatter of 0.044 nm.

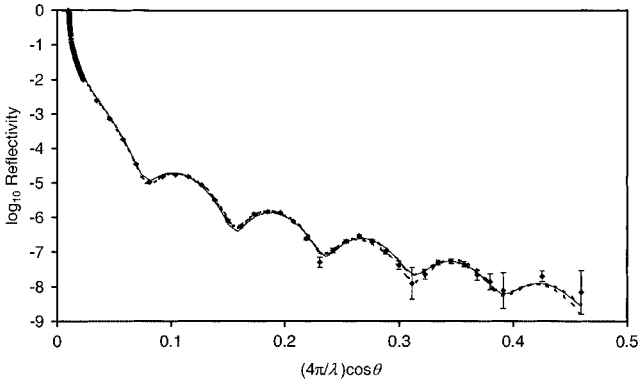

Figure 14. Neutron reflectometry response as a function of the momentum transfer $Q = 4\pi \sin\theta/\lambda$ for the 8 nm oxide on Si(100) measured at NIST, with the best fit (———) and two acceptable but poorer fits (- - - -).

It is expected that the GIXRR and neutron reflectometry data should give the highest accuracy but we note in Table 10 that, although the GIXRR results have m values close to the average for the other methods, the c values are close to the values for MEIS, NRA and RBS that measure the total oxygen. It is not clear why this is so and it may simply be that an adsorbed water layer, as distinct from carbonaceous contamination, looks like 0.5 nm of oxide.

Transmission electron microscopy

Transmission electron microscopy studies, like GIXRR and neutron reflectometry, provide a direct length measurement but here it is from the image of the cross-section of the film in which the pitch of the Si atoms using, for instance, the (100) planes at 0.5431021 nm is a traceable calibrant. The atomic spacing in silicon at 22.5 °C, *in vacuo*, is known to an accuracy of much better than 0.1 ppm,[94] which is far better than is needed here. It is this simple scaling that makes TEM so attractive. However, the difficulty in preparing samples means that data sets were often for less than the full ten samples.

The TEM studies were made either by conventional high-resolution TEM (HRTEM) or by scanning TEM (STEM). These differ in that usually in HRTEM the undiffracted transmitted electrons are detected and much of the contrast concerns coherent mechanisms arising from diffraction and interference effects. This leads to complications of contrast inversion with sample thickness. In STEM, a different mode can be realized by detecting electrons scattered through large angles on a high-angle annular detector in the dark field. This mode is called high-angle annular dark-field (HAADF) STEM. The contrast now arises from incoherent scattering and so avoids the contrast reversals with thickness and other coherent effects. The scattering contrast now depends more strongly on the atomic number Z of the atoms in the image field.[25] A further advantage is that the resolution in STEM is less affected by the sample thickness and so samples are easier to prepare. In the first HRTEM study from the PTB, measurements were made for the 2 nm and 4.5 nm oxides on (100) substrates. The results of the fits of these two results with the NPL data are given in Table 11. These data were originally recorded to evaluate the likely carbonaceous contamination correction for the ellipsometry data reported by the PTB.

The second set of TEM data is from BAM. Conventional TEM using orientation contrast only was applied for the measurements. The main problem with TEM is to get good contrast from, and to protect, the outer SiO_2 surface during the thinning process in order to manufacture the TEM cross-section. This thinning is typically to 100 nm to see through the sample. Here, the samples were coated with 10 nm of Ti and 40 nm of Pt by electron beam evaporation. For the preparation of thin cross-sections, face-to-face gluing, mechanical thinning and ion beam thinning with glancing-incidence Ar ions were used. Calibration of the microscope was made using the (111) fringes of Si in the high-resolution mode and by using the MAG*I*CAL calibration sample.[95] These

Table 11. The TEM results

Laboratory	Method, capping	m	c (nm)	r (nm)	Repeatability (nm)
PTB	HRTEM	0.913	0.734	—	—
BAM	HRTEM, Ti	0.851	1.064	0.232	0.096
Philips	HRTEM, Al	0.971	0.389	0.208	0.228
KRISS	HRTEM, Si	0.898	0.404	0.187	0.089
EMPA	HRTEM, Au	0.995	1.323	—	—
Daresbury Laboratory	HAADF-STEM, epoxy	1.072	0.537	—	—
Bell Laboratories	HRTEM, Ti	0.750	1.215	0.115	0.510
Bell Laboratories	HAADF-STEM, Ti	0.868	0.770	0.114	0.356
Average		0.915	0.804	0.171	
SD		0.099	0.361		

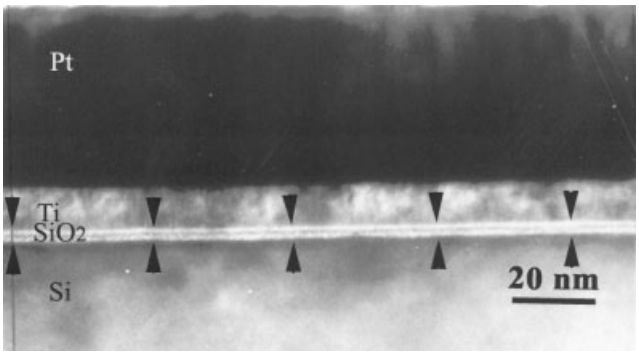

Figure 15. A TEM section of 2 nm (100) material with Ti and Pt capping by BAM. The scale marker is the instrument marker, which reads 3–4% lower than the calibrated value.

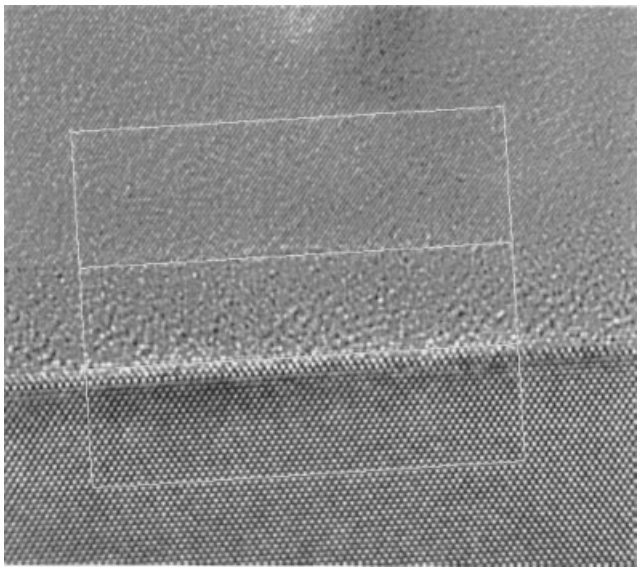

Figure 16. A TEM section for the 5 nm (100) material capped with Al and analysed using the parallel box method at Philips.

two methods gave magnifications that differed by <0.2%. The MAG*I*CAL thicknesses are traceable to the ⟨111⟩ lattice spacing of Si. Figure 15 shows an example for the 2 nm (100) material, indicating how five measurements were made in one locality. The results were measured using the original negative at an optical magnification of 10. The accuracies depend on the sharpness of the contrast changes at both interfaces, and these varied from sample to sample. Measurements were made for the 2, 4.5 and 8 nm (100) samples only. The standard deviations in these cases, from the repeat measurements, were 0.134, 0.100 and 0.055 nm. The m, c and r values from the data from the fit to the NPL thickness measurements are given in Table 11. Later additional measurements with the 2, 4, 6 and 7 nm (111) samples revealed the same trend, namely accurate determination for layer thicknesses >4 nm but large uncertainties for thinner layers. It should be mentioned that this problem arises because of both the amorphous nature of the SiO_2 layer and, probably, the contamination on the SiO_2 surface.

In the third TEM study at Philips the samples were thinned by mechanical polishing. To protect the surface and provide a crystalline overlayer so that the surface position an be identified accurately, a layer of Al was deposited within 1 h of opening the wafer container. The composite sample then was glued to a glass coverslip and the sample was thinned down to electron transparency, i.e. no additional ion milling was used. Aluminium is preferred to a heavy metal such as Pt because artefacts may be caused with Pt in polishing. The TEM imaging was made in a TECNAIF30 ST 300 keV instrument at a magnification of 800 000 using energy filtering to select electrons that have suffered no energy losses. The image scales were determined from the Si lattice using a Fourier transform approach with a standard uncertainty, evaluated from many measurements, of 0.6%. Measurements were made by fitting parallel lines to the interface over 70% of the field of view for three or more images for each sample in order to estimate the uncertainty of measurement, as shown in Fig. 16. Precise fitting of the lines by eye by two different operatives led to values differing by typically 0.1 nm. The SiO_2/Si interface was taken to be a line between the outer row of substrate Si atoms and the amorphous SiO_2. The standard deviations of the sets of measurements for each sample ranged between 0.05 and 0.39 nm. The m and c values for the fit of these data to the NPL thickness data are given in Table 11. These show an m value closer to unity and c closer to zero than the other TEM results. The r value is less than the repeatability because the fits are based on the averages of several measurements for

each sample. This set of data for TEM uniquely covers both the (100) and (111) samples. If we focus on the (100) samples, the m, c and r values in Table 11 should be replaced by $m = 1.000$, $c = -0.115$ nm and a lower r value of 0.117 nm.

The fourth set of TEM data is from KRISS. A similar gluing and thinning approach to that used at BAM was used here. Because the contrast between the glue and the SiO_2 is very poor, the samples were first capped with 250 nm of polycrystalline Si. The samples were analysed in a Hitachi H9000-NAR microscope working at 300 keV, with a point resolution of 0.18 nm and a lattice resolution of 0.1 nm. The average thicknesses were determined statistically from the image from the [110] zone axis of the Si substrate. Ten determinations were made for each of the (100) samples. The lower oxide interface is located by the last detectable dot of the intersecting 111 lattice fringe and the upper oxide interface by the termination of 111 lattice fringes. The average standard deviation of the ten measurements for each samples was 0.283 nm and the standard deviation of the mean thicknesses was 0.089 nm. The m, c and r results for the fit to the NPL thickness data are given in Table 11.

In the fifth set of data from EMPA, 4.5 and 8 nm (100) samples were analysed using a Philips CM30 transmission electron microscope working at an acceleration voltage of 200 kV. To provide contrast, the samples were capped with 30 nm of plasma vapour-deposited Au followed by a further protective layer of Pt. The samples then were prepared by focused ion beam (FIB) cutting and lifting. The contrast in these samples was excellent and allowed the separate regions to be identified clearly. The thicknesses were measured from interface to interface by eye with a ruler, leading to an uncertainty of 3% at each interface. Unfortunately, the Si lattice was not resolved due to the high thickness of the samples. Amorphization by the FIB may add further fuzziness to the image. The main uncertainty arises from the lack of clearly defined interfaces and here the fuzziness leads to an uncertainty of 15% in the film thickness. The total standard uncertainty is thus estimated at 16%. The m and c results for the fit to the NPL thickness data are given in Table 11. Because there are only two data points, there is no value for r.

In the sixth set of data from Daresbury Laboratory, the cleavage method of Lu *et al*.[12] was tried but was found unsuitable for standard wafer thicknesses and so the samples were glued face to face and thinned by polishing and low-angle ion milling. The TEM samples were investigated in an aberration-corrected STEM VG HB501 instrument at 100 keV electron energy. The HAADF image is formed by collecting high-angle-scattered electrons with an annular dark-field detector in a scanning transmission electron microscope with a collection angle range of 70–210 mrad. The contrast of HAADF images is strongly dependent on the average atomic number of the scattering atoms, is not strongly affected by dynamic diffraction effects, is not strongly affected by defocus and is not strongly affected by sample thickness variations. The spatial resolution is not as good as conventional high-resolution electron microscopy (HREM) but is still adequate for these purposes. Samples of the 2 nm and 4.5 nm (100) material were selected because Daresbury Laboratory was only invited to participate late in the study. These samples were baked several times by placing them for 7–10 min ~2 cm above a 50 W halogen bulb to prevent carbon contamination during electron beam illumination. For the 4.5 nm (100) material this was not sufficient. In that case, the area of interest was illuminated for ~30 min by the (under-focused) electron beam, with no apertures selected, in order to fix the contaminating carbonaceous material. After imaging, intensity profiles were obtained and the length scale was calibrated from the Si lattice. The oxide thickness was determined from the half-heights of the two slopes characterizing the surface and the interface, respectively. The m and c data from the fits of these data to the NPL thicknesses are given in Table 11.

In general, the SiO_2 layer is easily distinguishable from the bulk Si. However, determination of the layer thickness presents some difficulties. A phenomenon often encountered in the HAADF images is a broad ridge in the intensity distribution of the image along the SiO_2/Si interface.[96] This has been seen also by other investigators. There are different possible explanations for such a phenomenon and, depending on the interpretation, the interface position may be changed, leading to a different value of c.

The seventh, eighth and ninth sets of data are from Bell Laboratories and involve five of the (100) samples. Even though TEM is, in principle, the most direct method for measuring the thickness of a gate oxide, there are two weaknesses to the method that can lead to systematic errors that are difficult to estimate.

The first problem is a consequence of viewing electrons that have been transmitted through the thin sample. The silicon/oxide interface is viewed in projection and details along the projected direction are combined. For an atomically abrupt interface this would not be a problem but most thermal oxides (even those grown on atomically flat single terraces) exhibit an interface roughness in the range 0.13–0.3 nm. If the roughness profile is Gaussian, then at the very least the effect is to convolve the atomically abrupt interface with a Gaussian whose FWHM is 2.35σ or 0.3–0.7 nm per interface. When the imaging mode of the microscope is taken into account, the problem becomes more complicated. A conventional transmission electron microscope without the benefit of a through-focal series reconstruction is extraordinarily insensitive to roughness, heavily weighting the image towards the crystalline components, where the electron phases reinforce each other over the amorphous regions where the phases are scrambled.[97,98] In thicker samples, along the projected direction the roughness can be recognized as a black band.[99,100] Annular dark-field imaging, which is essentially incoherent in nature, does not suffer from this problem and the projected potential is faithfully reproduced in thin sections. In thick sections, the beam spreading in the crystalline and amorphous regions becomes asymmetric, making it more difficult to locate the midpoint.

The main issue is to define the effective positions of the surface and the interface of the SiO_2. Traditionally, electron microscopists have ignored this problem, and simply measured the extreme points, probably underestimating the

oxide thicknesses. Annular dark-field imaging is sufficiently quantitative for thin sections that a roughness profile, represented by the integral of a Gaussian function, can be fitted to the projected profile for each interface. Both the interface locations and the roughness profile convolved with the probe width then can be extracted.[98] Alternatively, the oxide width can be defined as the distance between the inflexion points at each interface. For a Gaussian roughness the two methods are equivalent. Here, we define the oxide width as the distance between the two inflexion points. It should be noted, however, that for noisy images this method has a tendency to overestimate the oxide thickness—the oxide signal is less than the silicon signal and potentially can become lost in the noise floor or accidentally clipped if the black level is not properly set. If the electron probe has substantial tails, then correcting for the probe shape by deconvolving the image with the known probe shape using a Richardson–Lucy algorithm[101,102] will not shift the position of the interface but it will reduce the uncertainty in its position.

The second problem is the need to add a capping layer. This introduces its own complications. The attempts at adding a Pt capping failed because the adhesion was too poor to survive the mechanical thinning to prepare a cross-section. Materials that stick well to oxides do so because they form strong bonds. This reaction is not necessarily limited to one atomic layer. From experience at Bell Laboratories, adding silicon to an uncapped oxide usually results in an additional 0.5 nm of silicon oxide (this was checked by synchrotron x-ray reflectivity of samples before and after capping). The most likely origin of the extra oxide is the silicon reacting with water or hydroxide groups on the oxide surface.

For the above reasons, a Ti capping layer was used. Because TiO_2 has a substantially different density to SiO_2, these would be relatively simple to distinguish. There is a risk, however, that the Ti may reduce the surface of the SiO_2, leading to a systematic underestimate of the SiO_2 thickness. This error, if present, does not seem to be >0.5 nm because no obvious TiO_2 phase was detected at the interface.

There are two imaging modes employed in this study. In conventional TEM the sample is illuminated with an incoming plane wave of electrons, which is recorded in parallel on a CCD after scattering through the sample. This image is dominated by phase contrast. Thickness changes and image defocus can lead to contrast reversals in the image. Consequently, quantitative analysis of a single image is challenging. The situation is substantially improved if a through-focal series can be collected and an exit-wave reconstruction is performed,[96,103] although here only a single-defocus image was recorded.

The second imaging mode is STEM. Electrons scattered in the forward direction can be analysed with an energy-loss spectrometer or recorded on a bright-field detector. Electrons scattered to large angles are collected with an annular dark-field detector. This signal is largely incoherent, dominated by amplitude contrast and not subject to contrast reversals. However, contrast can be reduced in thick samples due to beam spreading. Nevertheless, in thin sections the signal can be analysed quantitatively. The inner angle for the annular dark-field detector at Bell Laboratories was 45 mrad at 200 kV, corresponding to a scattering vector of 3.6 inverse angstroms. At 100 kV the equivalent angle would be 66 mrad. This is very similar to Daresbury Laboratory, where the inner angle of 70 mrad at 100 kV corresponds to a scattering vector of 3.8 inverse angstroms.

A JEOL 2010F instrument operating in STEM mode was used to record the images.[104] The microscope was fitted with an analytical ($C_s = 1$ mm) polepiece, JEOL annular dark-field detector, Fischione PEELS-compatible HAADF detector, Gatan imaging filter and bright-field/annular dark-field detectors. The STEM unit was controlled by a Gatan Digiscan system that allowed for two signals to be recorded simultaneously. By altering the camera length of the microscope, both HAADF and low-angle annular dark-field (LAADF) images could be recorded simultaneously, or HAADF and bright-field images or HAADF and electron energy-loss spectroscopy measurements could be made. The bright-field images are related by the principle of reciprocity to the phase-contrast images formed in TEM. The collection angle in STEM would correspond to the illumination angle in TEM.

Line profiles through the oxide were taken perpendicular to the interface and at least five unit cells wide. Between 10 and 20 independent profiles were taken from each sample. The oxide thickness was measured from the inflexion points at the interfaces in the annular dark-field images. This is not possible in the bright-field images so, instead, the extremity of the crystalline region is taken as the interface.[105]

Finally, a 1 nm thick band of amorphous carbon was detected on top of the 2 nm SiO_2 layer. This sample proved very difficult to cross-section and, not surprisingly had poor adhesion to the Ti capping layer. Results were first recorded for uncapped samples using STEM with annular dark-field detection but these were considered less reliable. Next conventional TEM and HAADF-STEM analyses were made and the fits of these are given in Table 11. In each case, the 2, 3, 4.5, 5 and 8 nm (100) samples were used. Note that in Table 11 the repeatability appears to be greater than the value of r. This arises because the values for the plot to give m and c use the average of many results, so here the repeatability of the mean is appropriate and this typically would be four times lower than the value given in Table 11. Because the scatter of the data varied markedly from sample to sample, the fits for m and c use weightings for each measured data point. Figure 17 shows results for the 8 nm (100) sample using HAADF-STEM. It is very clear that the central issue is still to define the interface position. The line profile provides a sensible and consistent analytical method that is probably better than the traditional judgements by eye. The 5 nm sample broke during preparation for the conventional TEM measurements and could have shown milling artefacts. By experience, it is felt that the HAADF-STEM results will be more accurate than conventional TEM on these capped samples.

These TEM results from Bell Laboratories agree with other measurements for the thicker oxides but show progressively greater thicknesses for the thin oxides. Concern about the reaction of Ti with SiO_2 (discussed above) or about

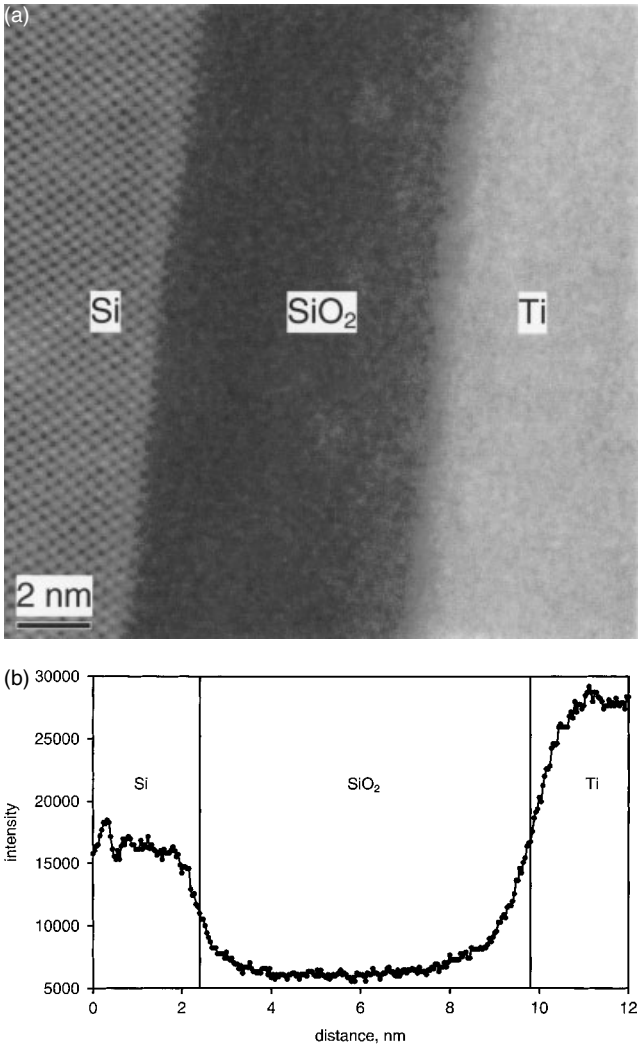

Figure 17. The TEM data from Bell Laboratories for the 8 nm (100) material capped with Ti and analysed using annular dark-field microscopy: (a) section clearly showing the Si lattice; (b) one of the ten line profiles showing the markers for the line profile, the average being 7.59 ± 0.11 nm.

the systematics of the methods of defining the interfaces should lead to a systematic addition or subtraction to the thicknesses for all oxides. Thus, if the other methods are correct m should be nearer unity and a positive or negative value of c may be found, depending on the preparation method. These TEM data generate m values that are lower than most other m values but in line with those by BAM, who also used Ti capping.

Diebold *et al*.[106] analysed the measurement of thin dielectric film thicknesses determined by TEM very carefully. In their assessment of data, the importance of exit wave reconstruction for aberration-corrected HRTEM and the selection of apertures for HAADF-STEM with deconvolved probe shapes in order to obtain meaningful images is shown. They propose that for reproducible film thickness determinations HAADF-STEM is used, with the thickness determined from intensity traces across the image using the method of Muller.[97] By reproducible, here, they mean reproducible by the one method between laboratories. This method is effectively shown in Fig. 17, relating to the data from Bell laboratories. In this work we have not tried to apply a recommended procedure for TEM but have left decisions to the individual analyst guided by their experience. Table 11 shows no significant difference between HRTEM and HAADF-STEM data here, with both leading to the same low value of m and high offset c. The data are all close to other methods for the thickest layer but are progressively offset for the thinner layers. The reason for this is not clear.

SOME GENERAL ISSUES OF UNCERTAINTY

The results have many different aspects that need consideration. Each of the methods is accurately linear but many involve input numbers that may differ from laboratory to laboratory and many involve contributions from the contamination layers or the outermost substrate layers. The data for each method thus need homogenization. We have not yet fully addressed all the issues of uncertainty because these issues only become clear when all the data are collected together. Many laboratories reported thickness values to one decimal place because they estimated the uncertainties as >0.1 nm. However, it was clear that many correlations were better than 0.1 nm and so data were requested to three decimal places in order to avoid rounding errors. This allows aspects such as the linearity of the methods to be evaluated accurately.

The most straightforward contributions to the uncertainty arise from the precision of the measurements that contribute to the type A uncertainties.[6] We first consider that the NPL XPS data have no uncertainty and then return to this issue later. The average value of r is 0.149 nm and the average repeatability is 0.13 nm, with about half below 0.1 nm in each case. Generally the value of r rises as the repeatability rises, because the value of r will have contributions from the repeatability, any variability in the individual sample contamination levels if it affects the measurements, the linearity of the method and of XPS with thickness, and the precision with which all the samples of a nominal thickness can be related to each other. Approximately, for these measurements in nanometres

$$r^2 \approx (\text{repeatability})^2 + (0.08)^2 \quad (16)$$

In most cases it is clear that the scatter of the data about the fit to the NPL data is random for the different samples. For the set of ten results (one for each sample) for an r value in nanometres independent of d_{SiO_2}, the standard uncertainties in the m and c values, S_m and S_c, are given by[107]

$$S_m = 17.6r\ (\%) \quad (17)$$

$$S_c = 0.791r\ (\text{nm}) \quad (18)$$

If, however, all 16 results are used (one for each sample and six further repeats for the 5 nm oxides), a slightly better result is obtained

$$S_m = 16.5r\ (\%) \quad (19)$$

$$S_c = 0.753r\ (\text{nm}) \quad (20)$$

About half of the data sets have 16 results and half have 10 results. Using the worst case, with an r value of 0.1 nm, the standard uncertainties of m and c are 1.8% and 0.08 nm, respectively. These errors are, of course, not uncorrelated. Because the data values are in the range 1.5–8 nm, there is an average, 2% decrease in m for a 0.08 nm increase in c.

We shall see, as we analyse the data, that some systematic uncertainties are significantly greater than these values but we now have the data to cross-calibrate to this level.

One issue that needs closer consideration is the value of the SiO_2 density. In a number of papers on optical measurements, models are used that involve changes in refractive index at interfaces or in zones close to the interface (see, for example, Ref. 108). These changes are a result of fitting programs and do not necessarily show a density change.[109] Measurements of bulk SiO_2 in different amorphous and crystalline forms show that the refractive index n and the density ρ are closely correlated.[24] From these data, over the density range 2.0–2.9 g cm^{-3}, the following relation can be derived

$$\rho = 5.33(n - 1.05) \tag{21}$$

This indicates that the refractive index may be used as a sensitive measure of the density; for a refractive index of 1.461, this gives a density of 2.191 g cm^{-3}. For fitting over the narrower density range 2.25–2.35 g cm^{-3}, the data give a density of 2.202 g cm^{-3} at this refractive index. The bulk density of amorphous SiO_2 (the form found in the thermal oxide) is given as 2.196 g cm^{-3},[23] which is within 0.3% of the values from Eqn. (21) and the fitting over the narrower range. Pliskin[110] previously had noted a similar result based on the Gladstone–Dale equation[111] and gave the result[112]

$$\rho = 4.785(n - 1) \tag{22}$$

from which the refractive index of 1.461 gives a density of 2.206 g cm^{-3}. Irene *et al.*[113] used the Lorentz–Lorenz formula

$$\rho = K(n^2 - 1)/(n^2 + 1) \tag{23}$$

where K is evaluated for a density of 2.212 g cm^{-3} at a refractive index of 1.462 for oxides grown at 1000 °C in dry oxygen. Studies of the refractive index of oxides grown on (100) and (111) substrates in dry atmospheres as a function of the growth temperature give refractive index values falling from 1.477 at 800 °C to 1.461 at >1200 °C, which Landsberger and Tiller[114] relate to densities falling from 2.270 to a final equilibrium value of 2.208 g cm^{-3}. They attribute the higher density at low temperature to unrelaxed compressive stresses arising from the growth mechanism. The present materials were grown at 800 °C because the heat treatment times become too short for practical growth of these thin oxides at higher temperatures.[27,28] However, for oxides thinner than 50 nm the growth process is via a faster mechanism than for thicker films, indicating that the relaxation issues that Landsberger and Tiller[114] consider for their 100 nm oxides are not relevant here and therefore that the final equilibrium density of 2.208 g cm^{-3} is appropriate. Other values for the density that have been determined are 2.21 g cm^{-3} by neutron reflectometry[13] and 2.24 g cm^{-3} by GIXRR.[13] From the refractive index data of Durgapal *et al.*[79] in establishing SiO_2 standard reference materials at NIST, n is found to be 1.461 at 632.8 nm wavelength. Using Eqn. (21) and the shorter fitting range we find densities of 2.191 and 2.202 g cm^{-3}, respectively, and using Landsberger and Tiller's data[114] a value of 2.208 g cm^{-3} is derived, averaging 2.200 g cm^{-3}. From the above seven values, a value of 2.208 ± 0.015 g cm^{-3} may be deduced where the standard uncertainty is 0.7% and covers the assumed value of 2.196 g cm^{-3} used earlier.

SUMMARY OF RESULTS

We start with an overall analysis for XPS. Figure 18 shows summary plots of m and c for the XPS data. Figure 18(a) shows the analysis for the reported XPS data and Fig. 18(b) shows the greater consistency from using common values for the parameters L_{SiO_2} and R_o. We see in Fig. 19 how this improves significantly on using the reference geometry and consistent values for L_{SiO_2} and R_o. It is clear from Fig. 19 that the average and standard deviation of the scatters of values give $m = 1.001 \pm 0.026$ and $c = -0.013 \pm 0.110$ nm, and using the reference geometry and consistent parameter values is excellent compared with the values of $m = 1.045 \pm 0.145$ and $c = 0.172 \pm 0.369$ nm for the initial results. This shows that instruments with very different designs and different x-ray sources, when operated with the reference

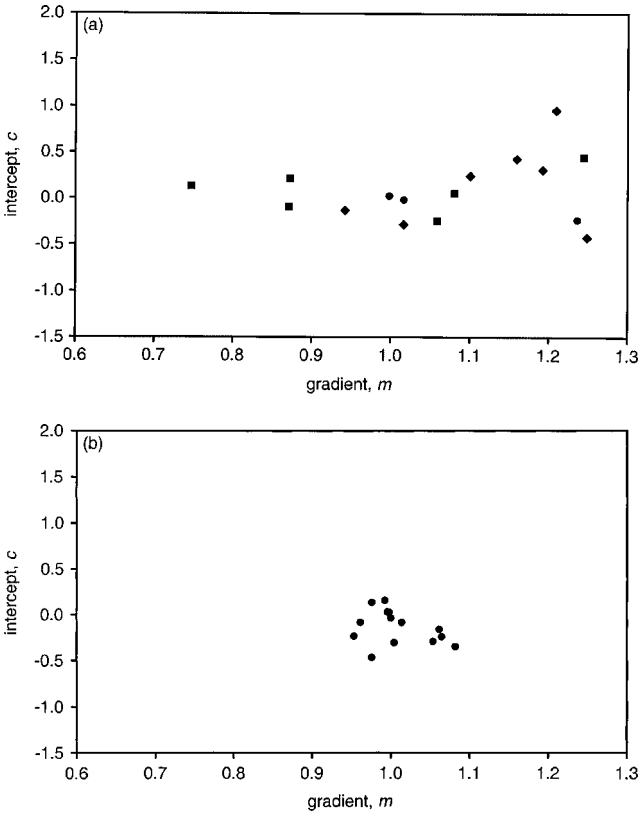

Figure 18. Plots of m and c for the XPS data using 0° emission (■), using ARXPS and fitting $\ln(1 + R_{expt}/R_o)$ versus θ to determine d (♦) and using single emission angles, not 0° (●): (a) as reported; (b) using the common values of $R_o = 0.9329$, L_{SiO_2} (Mg) = 2.964 nm and L_{SiO_2} (Al) = 3.448 nm.

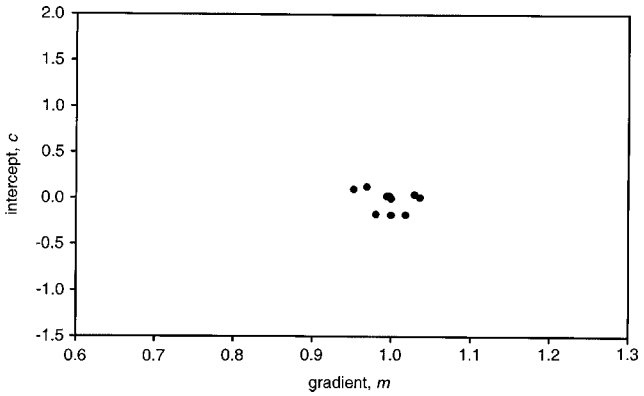

Figure 19. Plot of *m* and *c* for XPS with the reference geometry.

geometry and consistent L_{SiO_2} and R_o values, all give results that are consistent within the above standard uncertainties and that this gives an order of magnitude improvement in consistency compared with the use of local data and procedures. That the value of *m* is very close to unity is a matter of fortune because it depends linearly on the IMFP and here we have used calculated values with an estimated accuracy of 17.4%. The XPS data, however, have the unique attribute that the thickness should extrapolate linearly to zero at zero SiO_2 thickness, irrespective of the contamination. Small offsets occur for the methods using just the two peaks[6] arising from small non-linearity problems. These offsets are typically <0.02 nm.

In our earlier summary we found that the ellipsometry data sets gave an average of $m = 0.986 \pm 0.011$ at one standard uncertainty. This value is reliable because much work has been completed for thicker films where the optical constants have been very well established. However the offsets, *c*, reflect various contaminations. These offsets essentially have three values: the offset with new samples studied by the NPL was 0.480 nm; the average offset of other results without preheating was 1.016 ± 0.174 nm; and the average offset with preheating is slightly less at 0.871 ± 0.092 nm. The latter has reduced the contamination but has not eliminated it. This is precisely the effect observed by XPS at 260 °C but the remaining contamination then may be less easy to remove.[20,108]

The other data that should be consistent analytically are MEIS, RBS and NRA. For MEIS, using the SRIM-2003 values for dE/dx, $m = 0.953 \pm 0.040$ or as a standard deviation of the mean ± 0.020. This is consistent with the ellipsometry data. The offsets for oxygen using MEIS average 0.483 ± 0.108 nm. This represents the oxygen in the contamination layer. Very similar values appear for NRA and RBS, but with RBS the repeatability is rather poorer.

The interference methods of GIXRR and neutron reflectometry give average *m* values of 0.972 ± 0.003 and 0.991 ± 0.008, respectively. Neutron reflectometry, GIXRR and ellipsometry all have excellent traceabilities. The MEIS value of 0.953 ± 0.040 has an uncertainty of 4% in dE/dx and so the consistency with GIXRR and neutron reflectometry is good. The RBS value of 1.014 ± 0.064 has uncertainties in the individual contributions ranging from 3% to 10%. The results for these data are presented in detail in Fig. 20 and

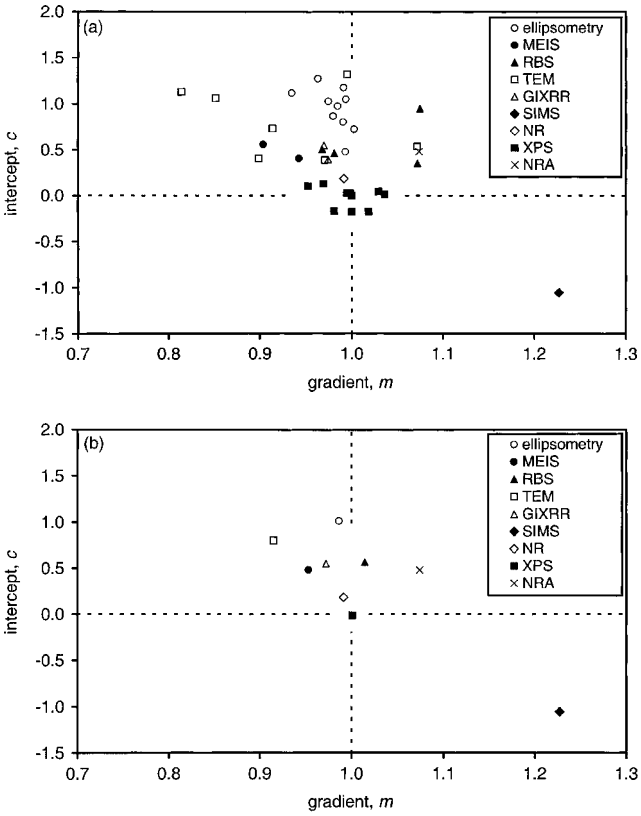

Figure 20. Plots of *m* and *c* for the homogenized data and for XPS with the reference geometry. The corrections used for surface contaminations in the footnotes to Tables 9 and 10 are not included here. This shows the direct result of applying the method: (a) for all of the data; (b) for the average values for each method, as shown in Table 13.

in Tables 12 and 13. Table 12 gives the averages and standard deviations for *m* and *c* for each method for the data as supplied by laboratories, and Table 13 shows these data corrected for the common density of 2.196 g cm^{-3} for thermal SiO_2. Also shown in Table 12 are the standard deviations of the means from the sets of data for each method, together with an estimate of the type B uncertainties at a level of 95% confidence. Table 14 shows some of the critical aspects of the traceabilities and the major uncertainties of the methods. The values of *c* all depend on the method, as discussed, but the values for *m* should all be the same. Taking each of the eight methods with equal weighting gives $m = 0.988 \pm 0.019$ for the 'as supplied' data and $m = 0.988 \pm 0.016$ for the homogenized data, where the uncertainties are the standard uncertainties for the value of *m*. Using weightings based on the reciprocal of the variances evaluated for the combined type A and type B uncertainties gives $m = 0.985 \pm 0.004$ for the 'as supplied' data and $m = 0.986 \pm 0.004$ for the homogenized data. For the weighted data, the strongest contributions arise from neutron reflectometry, GIXRR and ellipsometry. From the above results we take the weighted homogenized data to give $m = 0.986 \pm 0.009$ at a 95% confidence level with an expansion factor of 2.

If the above value for $m = 0.986 \pm 0.009$ is used, we may recalibrate the XPS data by reducing all of the XPS thicknesses. This may be done by accepting the R_o value of

Table 12. Summary Results for the average values of as-received data for *m* and *c* by method in ascending order of offset value with the standard deviation of the results and, in parentheses, standard deviations of the means arising from type A uncertainties ($B(m)$ and $B(c)$ are the type B uncertainties)

Method	*m*	$B(m)$	*c* (nm)	$B(c)$[b]
XPS	1.045 ± 0.145 (0.081)	0.175	0.172 ± 0.369 (0.069)	0.015
Neutron reflectometry[a]	0.991 ± 0.008 (0.008)	0.005	0.185 ± 0.050 (0.050)	0.005
NRA[a]	1.067 ± 0.041	0.031	0.477 ± 0.122	0.015
MEIS	0.921 ± 0.033 (0.017)	0.040	0.469 ± 0.119 (0.084)	0.100
GIXRR	0.972 ± 0.003 (0.002)	0.010	0.551 ± 0.004 (0.003)	0.000
RBS, EBS	1.006 ± 0.073 (0.030)	0.050	0.561 ± 0.266 (0.133)	0.050
TEM	0.915 ± 0.099 (0.035)	0.000	0.804 ± 0.361 (0.128)	0.000
Ellipsometry	0.986 ± 0.011 (0.004)	0.010	Preheat: 0.871 ± 0.092 (0.046)	0.200
			No preheat: 1.016 ± 0.174 (0.062)	0.200

[a] Only one result and so the standard deviation is calculated as described in the section on NRA and from the fit for *m* and *c*.

[b] Does not include effects of contamination.

Table 13. Summary results using homogenized data for the average values of *m* and *c* by method in ascending order of offset value with the standard deviation of the results and, in parentheses, standard deviations of the means

Method	*m*	*c* (nm)
XPS using reference geometry and NPL *L* and R_o values	1.001 ± 0.026 (0.009)	-0.013 ± 0.110 (0.037)
Neutron reflectometry[a]	0.991 ± 0.008 (0.008)	0.185 ± 0.050 (0.050)
NRA[a]	1.074 ± 0.013	0.480 ± 0.122
MEIS	0.953 ± 0.040 (0.020)	0.483 ± 0.108 (0.076)
GIXRR	0.972 ± 0.003 (0.002)	0.551 ± 0.004 (0.003)
RBS, EBS	1.014 ± 0.064 (0.026)	0.568 ± 0.263 (0.132)
TEM	0.915 ± 0.099 (0.035)	0.804 ± 0.361 (0.128)
Ellipsometry	0.986 ± 0.011 (0.004)	Pre-heat: 0.871 ± 0.092 (0.046)
		No pre-heat: 1.016 ± 0.174 (0.062)

[a] Only one result and so the standard deviation is calculated as described in the section on NRA and from the fit for *m* and *c*.

0.9329 and by scaling the previous values of L_{SiO_2} by 0.986 to give 2.923 nm for Mg x-rays and 3.400 nm for Al x-rays. At the reference geometry, by using these values XPS will have a standard uncertainty of 2.8%, mainly arising from the inconsistencies in the choices of the number of peaks to measure, from variations in the algorithms of the software used, from variations in the decisions on how to use that software and the earlier reference values for R_o and L_{SiO_2}. Greater consistency in the analysis of the peak areas may improve this further.

The above value of *m* may be used also to improve the accuracy of MEIS analysis by setting dE/dx equal to $0.953/0.986 = 0.967$ of the SRIM-2003 stopping power. This removes any bias but the 3.9% standard uncertainty between laboratories still remains.

Earlier we noted that the common density of 2.196 g cm^{-3} that we have used for SiO_2 may be replaced by a value of 2.208 ± 0.015 g cm^{-3}. This will reduce the thickness values obtained by MEIS, NRA and RBS and hence their *m* values by a factor of 0.9946. Changing the density to 2.208 g cm^{-3} reduces the weighted *m* value for the homogenized data from 0.9863 ± 0.0044 to 0.9859 ± 0.0044, and adding the uncertainty of 0.015 g cm^{-3} increases the standard uncertainty in *m* to 0.00 442. The uncertainty in the density thus has no significant effect on our overall conclusions, although it does affect specific data values. The density also will affect the value for XPS because the density used in the IMFP calculation was 2.19 g cm^{-3}.[33] This density effect may be evaluated from the generic IMFP equation, TPP-2M,[5] where the density appears explicitly in many terms and implicitly in the bandgap (E_g) value. The 0.7% uncertainty in the density leads to a 0.35% uncertainty in the IMFP (anticorrelated if E_g is fixed and correlated if E_g is set proportional to the density). This change is significantly less than the uncertainties listed in Table 13. We also noted that many of the analytical methods in principle gave thicknesses in terms of oxygen atoms m^{-2}. To derive these values, the parameters given earlier provide a conversion of 1 nm to 4.402×10^{19} oxygen atoms m^{-2}.

The offsets, *c*, have been discussed with each method and are shown visually in Fig. 21. There are three basic classes of offset: water and carbonaceous contamination equivalent to ~1 nm, as seen by ellipsometry; adsorbed oxygen mainly from water at an equivalent thickness of 0.5 nm, as seen by MEIS, NRA, RBS and possibly GIXRR; and no offset, as seen by XPS using the Si 2p peaks. Neutron reflectometry

Table 14. Critical aspects of the traceability of each method

Method	Essential traceability	Major uncertainty
MEIS	Calculated stopping powers	Stopping power, offsets
NRA	Integrated charge for reference sample	Parasitic currents, prior oxide on the sample
RBS	Rutherford cross-section, integrated charge, detector solid angle	Integrated charge, detector solid angle
EBS	Cross-section, beam energy, integrated charge, detector solid angle	Cross-section, beam energy
SIMS	Via any reference sample	Non-linearity in sputtering of outermost layers
XPS (RG)[a]	Attenuation length calculated or calibrated via other methods	Attenuation length
Ellipsometry	Optical data from bulk samples and length via stylus measurement	Validity of optical data
GIXRR	X-ray wavelength and x-ray optical data	X-ray optical data and contamination layers
Neutron reflectometry	Neutron wavelength and neutron optical data	Neutron optical data and contamination layers
TEM	Length via Si lattice	Defining interfaces

[a] RG = reference geometry.

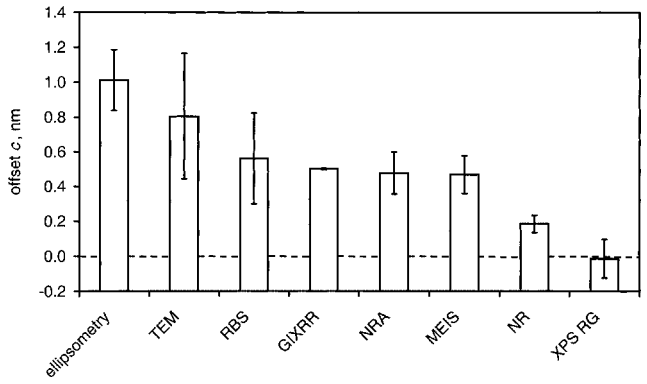

Figure 21. The offset *c*, shown as the average and standard deviation of the data in descending order of thickness. RG = reference geometry.

also gives a small but non-zero offset. The offset seen in TEM may arise as discussed above, and may therefore have a different origin. For MEIS, NRA and RBS, which measure the total oxygen, the average for the three methods is 0.510 ± 0.050 nm, with the standard uncertainty including the effect of the density, showing that it is the scatter within each method rather than the scatters between methods that generates the main contribution to the uncertainty. The value of 0.51 nm may be useful as a general offset to be removed when using these methods, to the extent that it is applied to similar wafers that have undergone a similar preparation and cleaning procedure.

The NRA and TEM data indicate some grounds for concern. It is not clear why the NRA data are almost 9% higher than the average data. In the TEM data there is a very clear traceability for the length scale but problems arise from three main sources: sample preparation, the selection of a very small region and identifying the accurate position of the interfaces. The concern arises because the average TEM value for *m* is 7% lower than that for the average data and the scatters in the *m* values from laboratory to laboratory are much higher than for other methods. The issues of sample preparation have been a major concern for many analysts because unreactive capping materials do not adhere well and reactive capping materials may reduce the outermost layer of the oxide, leading to thickness measures that are too low. If this is the case, the *m* values should still be correct but the *c* values will be negative. This may be the case for the Philips data but not for the remainder. Problems of bias in measuring the thickness at one locality have been overcome by using ten different samples for which, in many of the studies, many subsamples have been prepared and analysed. The remaining issue concerns the interface positions. It is noteworthy that at a thickness of 8 nm the TEM data agree with the average data. This indicates that there may be an unresolved uncertainty leading analysts to overestimate the thicknesses of layers in the 1.5–4 nm region by, typically, 0.6 nm.

Acknowledgements

The authors would like to thank the CCQM for approving this pilot study, Dr C. J. Powell for helpful suggestions in setting up the project, Dr P. J. Cumpson for assistance with the procurement and ellipsometry of the European samples and Drs C. R. Brundle, A. C. Diebold and R. M. Wallace for discussions on ultrathin oxides. This work is supported by the National Measurement Policy Unit of the UK Department of Trade and Industry and by separate funding sources in each of the participating laboratories. The authors would like to thank the following for assistance in conducting this work: P. L'Ecuyer, S. Tougaard, J. G. M. van Berkum, C. Cohen, P. Mantel, M. Hoffmann, W. E. S. Unger, D. Treu, H. Rooch, I. Kojima, T. Shiratori, T. Watanabe, H. Ando, A. Tanaka, H. Yoshikawa, Yong Jai Cho, Z. Q. Mo, O. Kenny, S. K. Tan, K. L. Yeo, S. W. Poon, M. van Staden, P. Gasser, T. C. Q. Noakes, C. Mulcahy, A. Bleloch and J. Grazul.

REFERENCES

1. *International Technology Roadmap for Semiconductors* (2001 and 2002 editions). http://public.itrs.net/
2. Tanuma S, Powell CJ, Penn DR. *Surf. Interface Anal.* 1991; **17**: 911.
3. Powell CJ, Jablonski A. *J. Phys. Chem. Ref. Data* 1999; **28**: 19.
4. Powell CJ, Jablonski A. *Surf. Interface Anal.* 2000; **29**: 108.
5. Tanuma S, Powell CJ, Penn DR. *Surf. Interface Anal.* 1994; **21**: 165.
6. Seah MP, Spencer SJ. *Surf. Interface Anal.* 2003; **35**: 515.

7. Seah MP, Gilmore IS, Spencer SJ. *J. Electron Spectrosc.* 1999; **104**: 73.
8. ISO 21270 : 2003 *Surface chemical analysis—X-ray photoelectron and Auger electron spectrometers—Linearity of intensity scale*. ISO: Geneva, 2003.
9. Seah MP, Brown MT. *J. Electron Spectrosc.* 1998; **95**: 71.
10. CCQM, Consultative Committee for Amount of Substance—Metrology in Chemistry. http://www.bipm.fr/enus/2_Committees/CCQM.shtml
11. CIPM, Comité International des Poids et Mesures. http://www.bipm.org/enus/2_Committees/CIPM.shtml
12. Lu ZH, McCaffrey JP, Brar B, Wilk GD, Wallace RM, Feldman LC, Tay SP. *Appl. Phys. Lett.* 1997; **71**: 2764.
13. Richter CA, Nguyen NV, Dura JA, Majkrzak CF. *CP449, Characterisation and Metrology for ULSI Technology: 1998 International Conference*, Seiler DG, Diebold AC, Bullis WM, Shaffner TJ, McDonald R, Walters EJ (eds). AIP: New York, 1998; 185.
14. Cole DA, Shallenberger JR, Novak SW, Moore RL, Edgell MJ, Smith SP, Hitzman CJ, Kirchhoff JF, Principe E, Neiveen W, Huang FK, Biswas S, Bleiler RJ, Jones K. *J. Vac. Sci. Technol. B* 2000; **18**: 440.
15. Semak BS, van der Marel C, Tougaard S. *Surf. Interface Anal.* 2002; **33**: 238.
16. Chang HS, Yang HD, Hwang H, Cho HM, Lee HJ, Moon DW. *J. Vac. Sci. Technol. B* 2002; **20**: 1836.
17. Tougaard S. *Surf. Interface Anal.* 1988; **11**: 453.
18. Tougaard S. *Surf. Interface Anal.* 1998; **26**: 249.
19. Tougaard S. *QUASES-Tougaard: Software Package for Quantitative Analysis of Surfaces by Electron Spectroscopy*, version 5.0 (2002) and *QUASES-ARXPS: Software Package for Quantitative ARXPS*, version 1.01 2001; www.quases.com.
20. Seah MP, Spencer SJ. *Surf. Interface Anal.* 2002; **33**: 640.
21. Seah MP, Spencer SJ. *J. Vac. Sci. Technol. A* 2003; **21**: 345.
22. Kaye GWC, Laby TH. *Tables of Physical and Chemical Constants* (16th edn). Longman: Harlow, 1995.
23. Lide DR. *Handbook of Chemistry and Physics* (81st edn). CRC Press: BOCA Raton, FL, 2000.
24. Helms CR, Poindexter EH. *Rep. Prog. Phys.* 1994; **57**: 791.
25. Diebold AC, Venables D, Chabal Y, Muller D, Weldon M, Garfunkel E. *Mater. Sci. Semicond. Process.* 1999; **2**: 103.
26. Seah MP, White R. *Surf. Interface Anal.* 2002; **33**: 960.
27. Massoud HZ, Plummer JD, Irene EA. *J. Electrochem. Soc.* 1985; **132**: 2685.
28. Han C-J, Helms CR. *J. Electrochem. Soc.* 1987; **134**: 1297.
29. *Guide to the Expression of Uncertainty in Measurement*. ISO: Geneva, 1993.
30. Hollinger G, Himpsel FJ. *Appl. Phys. Lett.* 1984; **44**: 93.
31. Keister JW, Rowe JE, Kolodziej JJ, Nümi H, Tao H-S, Madey TE, Lucovsky G. *J. Vac. Sci. Technol. A* 1999; **17**: 1250.
32. Shirley DA. *Phys. Rev. B* 1972; **5**: 4709.
33. Tanuma S, Powell CJ, Penn DR. *Surf. Interface Anal.* 1991; **17**: 927.
34. Andersen HH, Ziegler JF. *The Stopping Power and Ranges of Ions in Matter*. Pergamon: Oxford, 1977.
35. *ICRU Report 49. Stopping Powers and Ranges for Protons and Alpha Particles*. 1993.
36. Moon DW, Lee HI, Kim HJ, Nishimura T, Kido Y. *Nucl. Instrum. Methods B* 2001; **183**: 10.
37. Kido Y, Koshikawa T. *J. Appl. Phys.* 1990; **67**: 187.
38. Ziegler JF. *SRIM-2003*, version 02. http://www.SRIM.org
39. Hayton DJ, Jenkins TE, Bailey P, Noakes TCQ. *Semicond. Sci. Technol.* 2002; **17**: L29.
40. Amsel G, Samuel D. *Anal. Chem.* 1967; **39**: 1689.
41. Amsel G, Nadai JP, d'Artemare E, David D, Girard E, Moulin J. *Nucl. Instrum. Methods* 1971; **92**: 481.
42. Amsel G, Nadai JP, Ortega C, Rigo S, Siejka J. *Nucl. Instrum. Methods* 1978; **149**: 705.
43. Pringle JPS. *J. Electron. Chem. Soc.* 1972; **119**: 482.
44. Seah MP, David D, Davies JA, Jackman TE, Jeynes C, Ortega C, Read PM, Sofield CJ, Weber G. *Nucl. Instrum. Methods B* 1988; **30**: 140.
45. Tesmer JR, Nastasi M. *Handbook of Modern Ion Beam Materials Analysis*. Materials Research Society: Pittsburgh, PA, 1995.
46. Andersen HH, Besenbacher F, Loftager P, Moller W. *Phys. Rev.* 1980; **A21**: 1891.
47. Mayer M. *SIMNRA User's Guide, Report IPP 9/113*. Max-Planck-Institut für Plasmaphysik: Garching, Germany, 1997.
48. Wätjen U, Bax H. *Nucl. Instrum. Methods B* 1994; **85**: 627.
49. Feldman LC, Mayer JW, Picraux ST. *Materials Analysis by Ion Channelling*. Academic Press: New York, 1982; 159.
50. Ziegler JF. *Handbook of Stopping Cross-sections for Energetic Ions in All Elements*, vol. 5. Pergamon Press: New York, 1980.
51. Doolittle LR. *PhD Thesis*. Cornell University, Ithaca, NY, 1987.
52. Doolittle LR. *Nucl. Instrum. Methods B* 1985; **9**: 334.
53. Doolittle LR. *Nucl. Instrum. Methods B* 1986; **15**: 227.
54. Leavitt JA, McIntyre LC Jr, Ashbaugh MD, Oder JG, Lin Z, Desfouly-Arjomandy D. *Nucl. Instrum. Methods B* 1990; **44**: 260.
55. Cheng H-S, Shen H, Tang J, Yang F. *Nucl. Instrum. Methods B* 1993; **83**: 449.
56. Ziegler JF, Biersak JP, Littmark U. *The Stopping Ranges of Ions in Solids*. Pergamon Press: New York, 1985.
57. Barradas NP, Jeynes C, Webb RP, Wendler E. *Nucl. Instrum. Methods B* 2002; **194**: 15.
58. Jeynes C, Jalfri ZH, Webb RP, Kimber AC, Ashwin MJ. *Surf. Interface Anal.* 1997; **25**: 254.
59. Pascual-Izarra C, Bianconi M, Lulli G, Summonte C. *Nucl. Instrum. Methods B* 2002; **196**: 209.
60. Feng Y, Zhou Z, Zhou Y, Zhou G. *Nucl. Instrum. Methods B* 1994; **86**: 225.
61. Feng Y, Zhou Z, Zhou G, Yang F. *Nucl. Instrum. Methods B* 1994; **94**: 11.
62. Pauwels J. *CRM IRMM-302. Antimony Implanted in Silicon*. IRMM: Geel, Belgium.
63. Boudreault G, Jeynes C, Barradas NP, Wong KS. *Surf. Interface Anal.* to be published.
64. Lennard WN, Xia H, Kim JK. *Nucl. Instrum. Methods* in press.
65. Barradas NP, Jeynes C, Webb RP. *Appl. Phys. Let.* 1997; **71**: 291.
66. Jeynes C, Barradas NP, Marriott PK, Boudreault G, Jenkin M, Wendler E, Webb RP. *J. Phys. D: Appl. Phys.* 2003; **36**: R97.
67. Frost MR, Magee CW. *Appl. Surf. Sci.* 1996; **104/105**: 397.
68. Wittmaack K. *J. Vac. Sci. Technol. B* 2000; **18**: 1.
69. Tanuma S, Ichimura S, Goto K. *Surf. Interface Anal.* 2000; **30**: 212.
70. Kwei CM, Wang CY, Tung CJ. *Surf. Interface Anal.* 1998; **26**: 682.
71. Tougaard S. *J. Vac. Sci. Technol. A* 2003; **21**: 1081.
72. Powell CJ, Jablonski A. *J. Electron Spectrosc.* 2001; **114/115**: 1139.
73. Shallenberger JR, Cole DA, Novak SW, Moore RL, Edgell MJ, Smith SP, Hitzman CJ, Kirchhoff JF, Principe E, Biswas S, Bleiler RJ, Nieveen W, Jones K. http://www.eaglabs.com/offline/xpsiit2.pdf and *Proc. 12th Int. Conf. on Ion Implantation Technology*, Kyoto, Japan, Matsus J, Takaska G, Yamaha I Eds, vol. 1, 1998; 79, IEEE.
74. *NIST Standard Reference Database 82: NIST Electron Effective Attenuation Length Database*, version 1.0. NIST: Gaithersburg, MD.
75. Shallenberger JR, Cole DA, Downey DF, Falk S, Zhao Z. *Proc. 12th Int. Conf. on Ion Implementation Technology*, Kyoto, Japan, Matsus J, Takaska G, Yamaha I Eds, vol. 1, 1998; 566, IEEE.
76. *NIST Ellipsometry SRMs 2531 to 2536*, Office of Reference Materials, NIST: Gaithersburg, MD.
77. Pauwels J. *BCR-564*. IRMM: Geel, Belgium.
78. Tomkins HG. *A User's Guide to Ellipsometry*. Academic Press: New York, 1993.
79. Durgapal P, Ehrstein JR, Nguyen NV. *CP449, Characterisation and Metrology for ULSI Technology: 1998 Int. Conf.*, Seiler DG, Diebold AC, Bullis WM, Schaffner TJ, McDonald R, Walters EJ, (eds). AIP: New York 1998; 121.
80. Philipp HR. In *Handbook of Optical Constants of Solids*, Palik ED, (ed.). Academic Press: New York, 1985; 749.

81. Jellison GE Jr. *Opt. Mater.* 1992; **1**: 41.
82. Yasuda T, Aspnes DE. *Appl. Opt.* 1994; **33**: 7435.
83. Tu Y, Terstoff J. *Phys. Rev. Lett.* 2002; **89**: 86 102.
84. Azzam RM, Bashra NM. *Ellipsometry and Polarised Light*. North-Holland: Amsterdam, 1977.
85. Herzinger CM, Johs B, McGahan WA, Woolam JA. *J. Appl. Phys.* 1998; **83**: 3323.
86. Johs B. *SPIE Crit. Rev.* 1999; **72**: 29.
87. Krumrey M, Hoffmann M, Ulm G, Hasche K, Thomsen-Schmidt P. *Thin Solid Films*, to be published.
88. Kojima I, Boquan Li. *Rigaku J.* 1999; **16**: 31. http://www.rigakumsc.com/journal/index.jsp.
89. Parratt LG. *Phys. Rev.* 1954; **95**: 359.
90. Sinha SK, Sirota EB, Garoff S. *Phys. Rev.* 1988; **B38**: 2297.
91. Dura JA, Richter CA, Majkrzak CF, Nguyen NV. *Appl. Phys. Lett.* 1998; **73**: 2131.
92. Ankner JF, Majkrzak CF. *SPIE Proc.* 1992; **1738**: 260.
93. Sears VF. *Neutron News* 1992; **3**: 26.
94. 1998 CODATA Values, Mohr PJ, Taylor BJ. *J. Phys. Chem. Ref. Data* 1999; **28**: 1713; and *Revs. Mod. Phys.* 2000; **72**: 351. http://physics.nist.gov.
95. *MAG*I*CAL, JSM-001*. Structure Probe Inc.: West Chester, PA.
96. Yu Z, Muller DA, Baumann F, Silcox J. *Microsc. Microanal.* 2001; **7**: 186.
97. Kirkland EJ. In *Image and Signal Processing in Electron Microscopy*, Scanning Microscopy Supplement 2, Hawkes PW, Ottensmeyer FP, Saxton WO, *et al*. (eds). Scanning Microscopy International Chicago: 1988; 139.
98. Muller DA. In *Characterization and Metrology for ULSI Technology*, vol. 550, Seiler DG, Diebold AC, Shaffner TJ, *et al*. (eds). AIP: Gaithersburg, MD, 2000; 500.
99. Baumann FH, Chang C-P, Grazul JL, *et al. Mater. Res. Soc. Symp.* 2000; **611**: C4.1.1.
100. Muller DA, Neaton JD. In *Fundamental Aspects of Silicon Oxidation*, Chabal Y, (ed.). Springer: New York, 2001; 219.
101. Richardson WH. *J. Op. Soc. Am.* 1972; **62**: 55.
102. Lucy LB. *Astron. J.* 1974; **79**: 745.
103. Coene W, Janssen G, Op de Beck M, *et al*., *Phys. Rev. Lett.* 1992; **69**: 3743.
104. Muller DA, Grazul J. *J. Electron Microsc.* 2001; **50**: 219.
105. Kisielowski C, Principe E, Freitag B, Hubert D. *Phys. B* 2001; **308/310**: 1090.
106. Diebold AC, Foran B, Kisielowski C, Muller D, Pennycook S, Principe E, Stemmer S, *Microscopy and Microanalysis* 2003; **9**: 493.
107. Youden WJ. *Statistical Methods for Chemists*. John Wiley: New York, 1951.
108. Wang Y, Irene EA. *J. Vac. Sci. Technol. B* 2000; **18**: 279.
109. Hayzelden C. *Handbook of Silicon Semiconductor Metrology*, Diebold AC (ed.). Marcel Dekker: New York, 2001; 17.
110. Pliskin WA. *J. Vac. Sci. Technol.* 1977; **14**: 1064.
111. Gladstone JH, Dale TP. *Trans R. Soc (London)* 1863; **153**: 317, 337.
112. Pliskin WA, Lehman HS. *J. Electrochem. Soc.* 1965; **112**: 1013.
113. Irene EA, Tierney E, Angilello J. *J. Electrochem. Soc.* 1982; **129**: 2594.
114. Landsberger LM, Tiller WA. *Appl. Phys. Lett.* 1987; **51**: 1416.

APPENDIX

Addresses of institutes involved:

(1) Centre for Optical and Analytical Measurement, National Physical Laboratory, Teddington, Middlesex TW11 0LW, UK.
(2) ICPET, Nanostructured Material Group, National Research Council of Canada, 1200 Montreal Rd, Ottawa ON K1A 0R6, Canada.
(3) Groupe de Physique des Solides, Université de Paris 6 et 7, 2 Place Jussieu, 75241 Paris Cedex 05, France.
(4) Physikalisch-Technische Bundesanstalt (PTB), Arbeitsgruppe 5.15 'Quantitative Rastersondenmikroskopie', Bundesallee 100, D-38116 Braunschweig, Germany.
(5) Physikalisch-Technische Bundesanstalt (PTB), 7.12 Röntgenradiometrie, Abbestraße 2–12, D-10587 Berlin-Charlottenburg, Germany.
(6) Laboratory VIII.23, 'Surface & Thin Film Analysis', Bundesanstalt für Materialforschung und—prüfung (BAM), Unter den Eichen 44-46, D-12200 Berlin, Germany.
(7) Bundesanstalt für Materialforschung und -prüfung (BAM), V.1, Unter den Eichen 87, 12200 Berlin, Germany.
(8) Friedrich-Schiller-Universität Jena, Institut für Festkörperphysik, Max-Wien-Platz 1, D-07743 Jena, Germany.
(9) Abteilung Halbleiterphysik, Institut für Experimentelle Physik II, Fakultät für Physik und Geowissenschaften, Universität Leipzig, Linnéstrasse 5, 04103 Leipzig, Germany.
(10) Materials Characterization Division, National Metrology Institute of Japan, (NMIJ), AIST, AIST Tsukuba Central 5, Higashi 1-1, Tsukuba, Ibaraki 305-8565, Japan.
(11) Utsunomiya University, Yoto 7-1-2, Utsunomiya 321-8585, Japan.
(12) Center for Materials Analysis Technology, NTT Advanced Technology Corporation, Morinosato-Wakamiya, Atsugi, Kanagawa 243-0124, Japan.
(13) Materials Physics Group, National Institute for Materials Science, 1-2-2 Sengen, Tsukuba, Ibaraki 305-0047, Japan.
(14) Nano Surface Group, Materials Evaluation Center, Korea Research Institute of Standards and Science, Yusung PO Box 102, Taejon 305-606, S. Korea.
(15) Materials Evaluation Center, Korea Research Institute of Standards and Science, Yusung PO Box 102, Taejon 305-606, S. Korea.
(16) Optical Metrology, Photometry and Imaging Optics, Korea Research Institute of Standards and Science, Yusung PO Box 102, Taejon 305-606, S. Korea.
(17) PSB Corporation, 1 Science Park Drive, Singapore 118221.
(18) Surface Science Laboratory, Department of Physics, Faculty of Science, National University of Singapore, 2 Science Drive 3, Singapore 117542.
(19) Centre for Ion Beam Applications, Department of Physics, National University of Singapore, Singapore 119260.
(20) Materials Science and Characterization Laboratory, Institute of Materials Research & Engineering, 3 Research Link, Singapore 117602.
(21) Surface and Microanalysis, CSIR–National Metrology Laboratory (Meiring Naude Road/Brummeria), PO Box 395, Pretoria 0001, South Africa.
(22) Swiss Federal Laboratories for Materials Testing and Research (EMPA), Ueberlandstrasse 129, CH-8600 Dübendorf, Switzerland.
(23) Philips Centre for Industrial Technology, WY42, Prof Holstlaan 4, 5656 AA Eindhoven, The Netherlands.
(24) Philips Centre for Industrial Technology WAM 01, Prof Holstlaan 4, 5656 AA Eindhoven, The Netherlands.
(25) University of Surrey Ion Beam Centre, The Nodus Laboratory, Guildford GU2 7XH, UK.

(26) CLRC Daresbury Laboratory, Daresbury, Warrington WA4 4AD, UK.
(27) Cascade Scientific Ltd, ETC Building, Brunel Science Park, Uxbridge, Middlesex UB8 3PH, UK.
(28) SuperSTEM Laboratory, CLRC Daresbury, Cheshire WA4 4AD, UK.
(29) National Institute of Standards and Technology (NIST), Semiconductor Electronics Division, Gaithersburg, MD 20899, USA.
(30) Applied and Engineering Physics, Clark Hall, Ithaca, NY 14853, USA; formerly at Bell Labs, Lucent Technologies, 700 Mountain Avenue, Room 1E-356, Murray Hill, NJ 07974, USA.
(31) National Institute of Standards and Technology (NIST), Center for Neutron Research, 100 Bureau Drive, Mail Stop 8562, Gaithersburg, MD 20899-8562, USA.